Politecnico di Torino

Material Engineering for Industry 4.0

A.a. 2023/2024

March 2026

Synthesis & Characterization of Self-Healing Polymer Based on β-Amino Ester Covalent Adaptable Networks

Interpreting Steric and Chain-Length Effects

Supervisors:

Prof. Massimo Messori

Dr. Camilla Noe '

Candidate:

Amirhossein Mousavinia

ACKNOWLEDGEMENTS

I would like to thank *Dr. Camilla Noè* for her invaluable guidance, wisdom, and everything I have learned from her throughout this work. I am also very grateful to *Carlo di Bernardo* for his constant support and his precise scientific insights. I would also like to acknowledge *Marta Mollo* for her great help in performing many of the experimental tests. I extend my deep appreciation to *Prof. Massimo Messori* for creating such an inspiring and collaborative research group at Politecnico di Torino that truly broadens the horizons of science.

I am also deeply grateful to my family. I could never have reached this milestone without your constant love and support. A special thanks goes to my love, Fatima, for always being by my side and believing in me.

Finally, my thoughts and my heart remain with my homeland. It is my deepest, most enduring hope that **the dawn of true liberty will soon rise over my country**.

Table of Contents

List of figures

List of Tables

1 Abstract

The transition toward sustainable polymer materials necessitates overcoming the limitation of the end-of-life recycling inherent to traditional thermosets. Covalent adaptable networks (CANs) based on poly (β-amino esters) (PBAEs) offer a highly promising solution by uniquely exhibiting mechanistic duality, seamlessly transitioning between associative transesterification at moderate temperatures and dissociative aza-Michael exchange at elevated temperatures. This study reports the design, synthesis, and characterization of novel, structurally tunable, and catalyst-free PBAE CANs. A customized Michael acceptor, methacrylate triethanolamines (MATEOAs), was synthesized to provide built-in network branching and internal hydrogen-bond catalysis. Structural characterization of the synthesized MATEOA revealed a product dispersion mostly composed of tris- (70%), di- (7%), and mono-substituted fraction comprising 23% of the mixture. This monomer mix was formulated using a highly reactive, bio-based diamine (Priamine 1071) via aza-Michael addition. To systematically evaluate structure-property relationships, three macromonomers were incorporated into the base formulation: poly (ethylene glycol) diacrylate (PEGDA) of varying molecular weights (PEGDA-250 and PEGDA-700, respectively PG250 and PG700) and poly (ethylene glycol) dimethacrylate (PEGDMA-750, PGM).

Thermal, rheological, and mechanical characterizations revealed highly structure-dependent network properties. DSC identified optimum curing temperatures of 63 °C, 68 °C, and 74 °C for the PG250, PG700, and PGM formulations, respectively. Additionally, ATR-FTIR confirmed the successful transition from conjugated acrylates (1720 cm^{-1}) to saturated amino-esters (1740 cm^{-1}) alongside a competitive amide-formation pathway. In-situ rheological monitoring and solvent extraction demonstrated that PriMA-PG250 achieved controlled gelation (~40 min) and optimal structural integrity (84.1% gel fraction). Conversely, extending the aliphatic spacer (PriMA-PG700, 55.8% gel) yielded a looser network, while methacrylic substitution (PriMA-PGM, 31.3% gel) caused premature gelation (~10 min) and vitrification due to steric and electronic constraints. DMA and tensile testing indicated that chain extension lowered the α-transition (from -24 °C to -43 °C) and increased elongation at break to ~47%. Finally, stress-relaxation and 4-term Prony series modeling revealed that the densely cross-linked PriMA-PG250 exhibited high activation energy (E_a = 294.9 kJ/mol) and persistent solid-like behavior (G_∞ = 5.5%) at 180 °C. The flexible PriMA-PG700 and defective PriMA-PGM achieved total viscous flow (G_∞ ~0) at lower thresholds, demonstrating a highly tunable platform for reprocessable and sustainable vitrimers.

2 Introduction:

Modern society relies profoundly on polymeric materials, defining an era where daily life without plastics is virtually unimaginable; however, this technological advancement escalated into a global plastic pollution crisis.[1] Historically, addressing the diverse demands of material applications has relied on a fundamental division between two main classes of polymers: thermoplastics and thermosets. Thermoplastics are composed of entangled, linear polymer chains that can flow upon heating and dissolve in suitable solvents, facilitating their processability and recycling but often limiting their thermal and mechanical stability. Conversely, thermosetting polymers are characterized by a permanently cross-linked covalent architecture. While this three-dimensional network grants thermosets superior mechanical durability, dimensional stability, and chemical resistance compared to thermoplastics, it fundamentally prevents them from any reprocessability approach.[2] Consequently, at the end of their functional life cycle, thermosets are extremely challenging to recycle and are predominantly relegated to waste accumulation or incineration.[3] To overcome this inherent trade-off between the vital reprocessability of thermoplastics and the robust, stable performance of thermosets, the inclusion of dynamic covalent chemistry (DCC) into thermoset networks has recently gained attention.[4] By incorporating reversible covalent bonds into polymer matrices, a novel class of materials known as Covalent Adaptable Networks (CANs) has emerged, offering a promising pathway to design robust, cross-linked networks that can still be reshaped and recycled.[2,5,6]

The fundamental defining characteristic of CANs is that, while they are covalently cross-linked like traditional thermosets, their cross-linking points are designed to be reversibly cleavable in response to external stimuli[7] such as temperature fluctuations[8] or light irradiation.[9] Introducing these dynamic cross-links fundamentally expands the functionality of the polymer network; the ability of the network to rearrange over time imparts a unique viscoelasticity, a blend of solid-like and fluid-like properties, that enables advanced behaviors including moldability, injectability, and self-healing.[10] The foundational concept of dynamic covalent networks is not entirely new; decades ago, researchers observed thermally activated dynamic behaviors in cross-linked rubbers utilizing disulfide bonds[11] or silyl ethers.[12] However, CANs designed before 2010 primarily relied on a strictly detached mechanism, wherein existing chemical bonds had to be completely severed before new connections could be formed.[2,13] In recent years, scientific efforts have vastly expanded the library of applicable DCC, moving beyond early models to incorporate reversible cycloadditions,[14–16] transalkylation,[17–19] trans(thio)esterification,[20–22] transamination,[23–28] imine metathesis,[29] and much more.[24,30,31]

To fundamentally understand and tailor the behavior of CANs, they are primarily classified by their underlying crosslink exchange mechanism into two distinct categories: dissociative and associative networks.[10,31] In a dissociative process, the covalent crosslinks must first cleave into individual, reactive constituent partners; these released network segments must then diffuse until they encounter and bond with a complementary moiety to regenerate the crosslink.[31,32] Because this mechanism relies on discrete, sequential debonding and rebonding steps, dissociative networks characteristically exhibit a gel-sol transition at elevated temperatures, where the dissociation of bonds becomes entropically favorable.[10] Representative chemistries driving dissociative CANs include Diels-Alder cycloadditions,[14] hindered urea exchange,[33] boronate esters,[34] and various Michael-type additions.[35–38]

Conversely, associative CANs undergo dynamic exchange through a simultaneous addition-elimination sequence.[10] In this concerted process, a pendant reactive group within the polymer matrix reacts with an existing crosslink to form an intermediate species that eventually collapses into a newly formed crosslink. This peculiar behavior implies that bond breakage and formation occur in a single step.[31,32] Since the bonds never fully detach, associative CANs uniquely maintain a constant crosslink density throughout their network rearrangement.[31] This continuous connectivity inherently prevents a macroscopic gel-sol transition, imparts superior solvent resistance, and allows the material's stiffness to increase as a function of temperature due to entropic elasticity.[10]

Polymer networks that rearrange exclusively through this associative mechanism represented a breakthrough in the field, thanks to the pioneering work from Leibler et al. Such CANs were showing a flow behavior similar to that of vitreous silica and, hence, were named “vitrimers”.[22] Vitrimers' novel rheological profile showed a decrease in viscosity with increasing temperature. As a result, vitrimers typically maintain the robust insolubility characteristic of thermosets,[5] Yet they can be efficiently reshaped and recycled through simple heating without requiring the highly precise temperature control necessary for many traditional materials.[2] While transesterification remains the most prominent exchangeable chemistry for these associative vitrimers, the field has expanded to include transcarbonation, imine exchange, olefin metathesis, and the transamination of vinylogous urethanes.[31] Ultimately, while both dissociative and associative classes offer substantial molecular tunability and exhibit Arrhenius-like flow behavior, selecting between them requires a full consideration of the target application's specific operating conditions, environmental compatibility, and desired physical states.[10]

Despite the vast potential of CANs and vitrimers, a significant practical limitation is their frequent reliance on external catalysts, such as metallic salts or organic bases, to facilitate

and regulate the kinetics of network exchange.[39] The incorporation of these external agents often presents critical drawbacks, including the potential leakage of toxic compounds, catalyst migration and loss, and thermal decomposition, all of which can prematurely degrade the material and limit the number of viable reshaping and recycling cycles.[2] To circumvent these issues, researchers have increasingly prioritized the design of catalyst-free CANs. This can be achieved by utilizing inherently rapid exchange reactions, employing a large excess of exchanging functional groups, or leveraging molecular architectures that provide internal catalysis or neighboring group participation (NGP).[2,31,40] In NGP, nearby chemical substituents covalently interact with the reaction center during exchange to accelerate the reaction rate, whereas internal catalysis relies on longer-range effects such as electrostatic interactions or steric influences.[2]

Within this context of catalyst-free design, poly (β-amino esters) (PBAEs) have emerged as an exceptionally promising polymer architecture.[31] Historically investigated for biomedical applications due to their hydrolytic degradability and charge reversibility[41], PBAEs are easily and efficiently synthesized via the aza-Michael addition of a nucleophilic amine to an electron-deficient acrylate.[42] This synthesis shares highly advantageous features with click-chemistry, notably mild reaction conditions and high conversion rates. Crucially, aza-Michael reaction generates multiple tertiary amines along the polymer backbone, seamlessly providing the necessary internal environment to drive dynamic exchange without the need for external additives.[31] Furthermore, β-amino esters present a highly unique and intriguing profile among CANs: at elevated processing temperatures, they undergo dynamic bond exchange via associative and dissociative mechanisms simultaneously.[1,31,43] Given the simplicity of their synthesis, the vast commercial availability of amine and acrylate building blocks, and their inherent thermal responsiveness and degradability, PBAE-based networks represent a highly versatile, accessible drop-in technology.[4] They hold significant promises for overcoming the current processing and recycling limitations of traditional thermosets across diverse applications[1], ranging from photocurable coatings and adhesives to robust bulk biomaterials.[44]

Building upon the robust potential of catalyst-free poly (β-amino ester) networks, this work aims to design and synthesize a novel, highly reactive, and sustainable CAN utilizing carefully selected monomers. Central to this system is the development of tailored Michael acceptors: methacrylated triethanolamines (MATEOAs). By substituting the hydroxyl group of triethanolamine with a methacrylate moiety, the resulting monomer retains critical structural and chemical functionalities. The inherent tertiary amine structure within MATEOAs is structurally advantageous for generating a highly branched polymer architecture, while simultaneously providing reversibility.[31] Additionally, the tertiary

amine center serves a vital kinetic function for unreacted hydroxyl residues in the MATEOAs, representing a classic example of neighboring group participation (NGP).[45] The presence of a β-amine group was purposely designed to work as a potential internal catalyst towards transesterification, aiming to improve the overall reactivity via hydrogen bonding activation.[46] Mechanistically, the tertiary amine centers effectively enhance the nucleophilicity of surrounding free hydroxy groups to facilitate the dynamic transesterification, happening at higher temperature regimes compared to aza-Michael exchange.[47]

Priamine 1071 (Figure 1a) A fatty acid dimer-derived diamine was selected as the Michael donor for this study in virtue of its long, flexible aliphatic chains. Beyond enhancing the bio-content of the final material, Priamine 1071 exhibits exceptionally high reactivity. Previous studies have demonstrated that Priamine 1071 aza-Michael kinetics promote reaction initiation at ambient conditions, yielding full monomer conversion.[46] The synergistic combination of the MATEOA acceptors and the highly reactive Priamine 1071 donor, thereby, establishes an ideal foundation for synthesizing a functional, catalyst-free adaptable network.

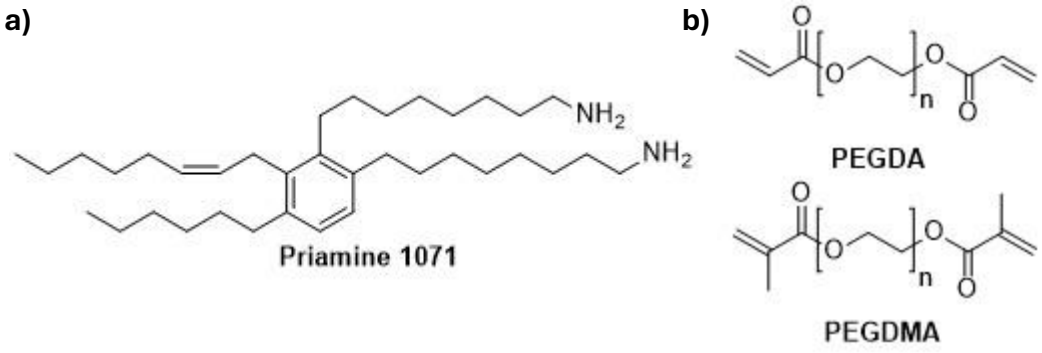

Figure 1. Priamine 1071, PEGDA, and PEGDMA structure

To precisely tune the thermomechanical and rheological behavior of the formulated system, our study introduces macromonomer, poly (ethylene glycol) diacrylate (PEGDA) and poly (ethylene glycol) dimethacrylate (PEGDMA) (Figure 1b). PEGDA co-monomers of varying molecular weights (PEGDA-250 $g.mol^{-1}$ and PEGDA-700 $g.mol^{-1}$) were incorporated to systematically assess how the length of the flexible spacer impacts the overall network mobility, crosslink density, and the efficiency of the dynamic exchange. This structural strategy is directly supported by previous research that reported fast-reprocessable epoxy CANs that can be achieved by the introduction of pendent aliphatic chains. Aliphatic chains insertion is a well-known strategy to improve the polymer segments' flexibility, retaining mechanical and thermal properties.[48,49] Concurrently,

PEGDMA-750 has been utilized to explicitly evaluate the steric and kinetic effects introduced by the methyl group on the methacrylate double bond, contrasting its behavior with the unhindered acrylate groups of PEGDA.

Ultimately, by integrating these systematically varied crosslinker segments into the synergistic, highly reactive MATEOA-Priamine networks, this work aims to elucidate the fundamental structure-property relationships governing these novel, catalyst-free poly (β-amino ester) vitrimers, paving the way for highly tunable and rapidly reprocessable materials.

3 Experimental Section

3.1 Materials

Triethanolamine (analytical RPE grade, > 97 %) was purchased from Carlo Erba Reagents. Methacrylic anhydride (> 98 %, contains 2,000 ppm Topanol A as inhibitor), sodium bicarbonate (> 99.5 %), chloroform (anhydrous, > 99 %, contains 0.5–1.0 % ethanol as stabilizer), poly (ethylene glycol) diacrylate (PEGDA, average M_n ~250), poly (ethylene glycol) diacrylate (PEGDA, average M_n ~700), and poly (ethylene glycol) dimethacrylate (PEGDMA, average M_n ~750, contains 900–1100 ppm MEHQ as inhibitor) were purchased from Sigma-Aldrich. PRIAMINE™ 1071-LQ-(GD) (Amines, C36-alkylenedi-, <100%) was kindly provided by Cargill. All reagents were used without further purification unless stated otherwise.

3.2 Preparation of Methacrylate Triethanolamines

Methacrylate triethanolamine mix (MATEOAs) was synthesized via the esterification of triethanolamine (TEOA) and methacrylic anhydride (MAAH) in an equimolar ratio (1:1), as illustrated in Scheme 1. The synthesis was conducted in two separate batches containing 0.234 mol and 0.177 mol of the reactants, respectively. For each batch, the calculated volumes of TEOA and MAAH were combined in a 250 mL round-bottom flask. Due to the high TEOA viscosity, the reaction mixture was manually mixed for 5–10 minutes to ensure homogeneity, followed by continuous magnetic stirring at room temperature over 24 hours.

The reaction flasks were kept in a water bath at room temperature to properly disperse heat build-up from the reaction.

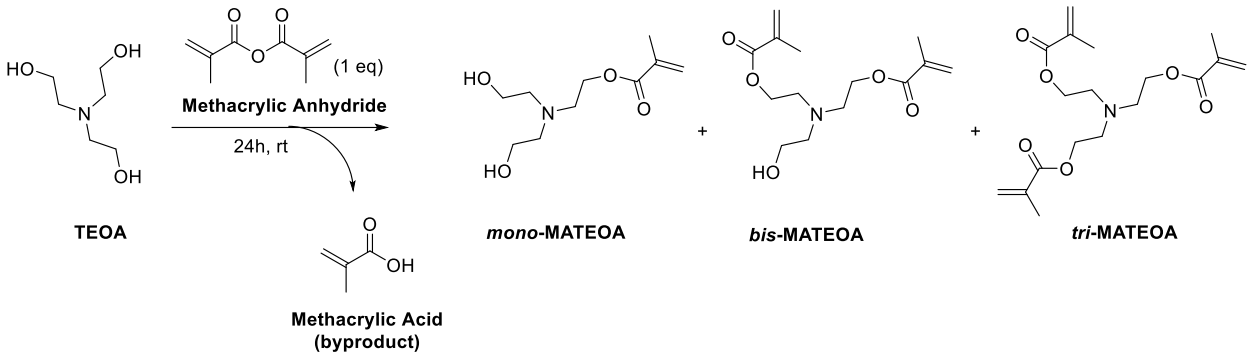

Scheme 1 Reaction scheme relative to METEOAs mix synthesis

Following the 24-hour reaction period, chloroform was added to the reaction mixture at a volumetric ratio of 1:1.5 (chloroform to reaction mixture, v/v) to prepare the organic phase for subsequent purification. The methacrylic acid (MAA) byproduct was neutralized and removed by a three-fold extraction, using a 5% w/w aqueous sodium bicarbonate ($NaHCO_3$) solution. A total volume of 690 mL of the $NaHCO_3$ solution (containing 34.524 g of $NaHCO_3$) was utilized, partitioned into approximately 390 mL for the first batch and 300 mL for the second batch, allowing for the successful separation of the chloroform-based organic phase.

$$0.411 \text{ mol} * 84 \text{ g/mol} = 34.524 \text{ g} * (100 \text{ ml} / 5 \text{ g}) = 690 \text{ ml} = 3* 130 \text{ ml} + 3* 110 \text{ ml}$$

The collected organic phases were then dried over anhydrous Na_2SO_4 to remove residual moisture and filtered by gravity. Chloroform was eventually removed under vacuum, yielding the isolated monomer mix. The isolated MATEOA product was stored under refrigeration to preserve its chemical stability before subsequent polymerizations.

3.3 Synthesis of PBAE-Based CANs

The PBAE-based CANs were synthesized via aza-Michael addition. The network formulations were meticulously designed based on a specific stoichiometric ratio of (meth)acrylate to primary amine moieties of 0.5:1 (corresponding to 2 equivalents of (meth)acrylate per 1 equivalent of primary amine).[46]

To establish a standardized batch scale, the formulations were calculated based on an initial 3.15 mmol of the synthesized MATEOA monomer. A 1:1 molar equivalence was maintained between the MATEOA acceptor and the selected macromolecular chain

extenders (PEGDA or PEGDMA). The required amounts for each component were determined using the following stoichiometric relationships:

- Moles of Extender:

$$n_{PEG} = n_{MATEOA} = 3.15\ mmol$$

- Total Acrylate Equivalents:

$$n_{Acrylate} = (2.47 * n_{MATEOA}) + (2 * n_{PEG}) = 14.08\ mmol$$

- Required Primary Amine Equivalents (based on 1:0.5 ratio):

$$n_{Primary\ Amine} = 0.5 * n_{Acrylate} = 7.04\ mmol$$

- Required Priamine 1071 (containing 2 primary amines per molecule):

$$n_{Priamine} = 0.5 * n_{Primary\ Amine} = 3.52\ mmol$$

The specific calculated mass amounts for each formulated samples, designated as **PriMA-PG250**, **PriMA-PG700**, **and PriMA-PGM**, are summarized in Table 1.

Table 1. Calculated formulation amounts for the synthesis of PBAE-based CANs (all amounts are in grams)

Sample name	*MATEOA*	*PEGDA 250*	*PEGDA 700*	*PEGDMA*	*Priamine 1071*
PriMA-PG250	1	0.787	-	-	1.992
PriMA-PG700	1	-	2.205	-	1.992
PriMA-PGM	1	-	-	2.3625	1.992

To prepare the cross-linked networks, a protocol adapted from the literature was employed.[1] The multifunctional MATEOA/PEGDA/DMA mix and the primary amino compound (Priamine 1071) were accurately weighed according to Table 1. The components were combined and thoroughly homogenized using continuous magnetic stirring for 2 minutes at room temperature. The well-mixed resin was then carefully poured into silicone molds of different geometries, avoiding air bubble formation.

To complete the network build-up, the molds were placed in an oven and cured at their respective optimum temperatures, for which the precise determination is discussed in the following sections. For the formulations containing standard acrylate (PriMA-PG250 and

PriMA-PG700), the curing process was conducted for 72 hours. However, the sample incorporating the methacrylic chain (PriMA-PGM) required a longer curing time of 7 days.

3.4 Characterization

Differential scanning calorimetry (DSC) measurements were performed using a DSC 214 Polyma (Netzsch, Germany) to evaluate the curing kinetics and thermal behavior of the uncured prepolymer mixtures. Samples weighing approximately 10 mg were analyzed under a continuous N_2 atmosphere. To determine the optimum curing temperature, dynamic scans were first conducted from 25 °C to 180 °C at three distinct heating rates (2.5, 5, and 10 °C/min) to evaluate the exothermic peak corresponding to the aza-Michael reaction. Subsequently, a second series of analyses was performed over an extended temperature range from −50 °C to 250 °C at a constant heating rate of 10 °C/min. This wider temperature sweep was utilized to accurately monitor the initial onset point of the curing process. Finally, to determine the thermodynamic glass transition temperature (T_g) of the fully cured networks, an initial heating scan from −50 °C to 170 °C at 10 °C/min was applied to each sample to relieve internal stresses and facilitate complete post-curing. Following a controlled cooling step to −50 °C at 20 °C/min, a second heating scan to 170 °C at 10 °C/min was conducted to accurately measure every thermal transition.

Rheological properties & Dynamic Mechanical Analysis (DMA) were characterized using MCR 702e MultiDrive (Anton Paar, Austria). To monitor the *in-situ* curing process, rheological *temperature sweeps* were conducted using parallel-plate geometry. The uncured resin was heated from 15 °C to 120 °C at a heating rate of 10 °C/min in air atmosphere in the linear viscosity region at a constant 0.1% shear strain. Throughout the experiment, the reactive gap was adjusted to avoid losing contact between material and plate. The evolution of the storage (G') and loss (G'') moduli was recorded over time. Following network formation, the solid-state *viscoelastic properties* of the cured samples were evaluated using rectangular specimens with approximate dimensions of 7 mm (L) × 5 mm (W) × 1.4 mm (T). The specimens were heated from −75 °C to 170 °C at a heating rate of 2 °C/min, and the glass transition temperature (T_g) of each network was determined from the maximum peak of the resulting tan δ curve. To quantitatively evaluate network connectivity, the apparent crosslinking density (υ_c, expressed in mol/m^3) was calculated using the following Equation:

$$\upsilon_c = E'/3RT$$

where E' is the storage modulus in the rubbery plateau [Pa], R is the universal gas constant (8.314 $J \cdot K^{-1} \cdot mol^{-1}$), and T is the absolute temperature in Kelvin. Finally, *stress-relaxation* experiments were performed to investigate the network bond exchange kinetics. A constant shear strain of 0.5% was applied to the material and the corresponding relaxation modulus, G(t), was recorded over time in isothermal temperatures regimes, from 200 °C to 100 °C. The activation energy (E_a) of the dynamic exchange process was calculated using characteristic relaxation times extracted both from time-temperature superposition (TTS) master curves (τ^*) and independently from the 1/e (approximately 37%) decay point of the normalized relaxation modulus (τ). Furthermore, mathematical fitting models were applied to the stress-relaxation profiles to quantitatively interpret the complex viscoelastic behavior and structural dynamics of each formulation.

Thermogravimetric analyses were performed using TGA-SDTA 851 (Mettler Toledo, USA) to evaluate the thermal stability and degradation behavior of the cured PBAE networks. Measurements were conducted on samples weighing approximately 10 mg in air atmosphere. The thermal degradation profiles were recorded in dynamic mode by heating the samples from 30 °C to 1000 °C at a constant heating rate of 10 °C/min.

Attenuated total reflectance Fourier transform infrared (ATR-FTIR) spectra were recorded using a Nicolet Thermo Fisher FTIR spectrometer equipped with an ATR module. The spectra were collected over a broad wavenumber range from 4000 to 400 cm^{-1} at 32 scans with a high spectral resolution of 4 cm^{-1}. Prior to sample analysis, a background spectrum of the clean ATR crystal was collected and used as a reference to ensure accurate peak determination. The recorded spectra were subsequently baseline-subtracted.

The gel fraction of the cross-linked networks was determined using a solvent-extraction method in accordance with ASTM D2765-16.[50] First, the cured specimens were accurately weighed to record their initial mass (W_i). The samples were then fully immersed in chloroform for 24 hours to extract any unreacted monomers or soluble fraction, as non-cross-linked oligomers. After the extraction period, the swollen specimens were removed from the solvent and dried under a laboratory fume hood for 3 hours. Subsequently, the samples were placed overnight at 80 °C in an oven to ensure the complete removal of any residual chloroform. Finally, the dried samples were weighed again to record their final mass (W_f). The gel content percentage was calculated using the following equation:

$$Gel\% = \left(1 - \frac{Wi - Wf}{Wi}\right) * 100$$

where W_i is the initial weight of the cured sample prior to immersion, and W_f is the final weight of the dried sample after the extraction process.

The mechanical properties of the synthesized networks were evaluated under uniaxial tension mode. Dog-bone-shaped specimens were prepared, featuring a rectangular gauge section with a useful length of ~ 25 mm, a width of ~ 3.5 mm, and a thickness of roughly ~ 0.3 mm. The tensile stress-strain measurements were performed at room temperature using an INSTRON universal testing machine (Ulm, Germany) with a constant crosshead velocity of 2 mm/min. The samples were stretched until complete failure to determine the Young's modulus, ultimate tensile strength, toughness, and elongation at break.

4 Results and Discussion

4.1 Synthetic Approach to MATEOAs monomer mix

The synthesis of methacrylated triethanolamines (MATEOAs) was carried out via the esterification of triethanolamine by methacrylic anhydride (MA). The synthesis was designed to achieve a mix of *tris*-, *bis*-, and *mono*-functionalized TEOAs to avoid the total TEOA grafting. In doing so, extensive ^{1}H-NMR analyses were previously carried out in the Polymer and Technology Group (*Department of Applied Science and Technology,* DISAT) to target a proper TEOA/anhydride ratio that could yield TEOA monomers still bearing free -OH functionalities. Eventually, the ratio employed in this study was selected to be TEAO:MA of 1:1. As illustrated in Figure 2, The final monomer mix was predominantly composed of *tris*-MATEOA at 70%, alongside 7% *bis*-MATEOA and 23% *mono*-MATEOA.

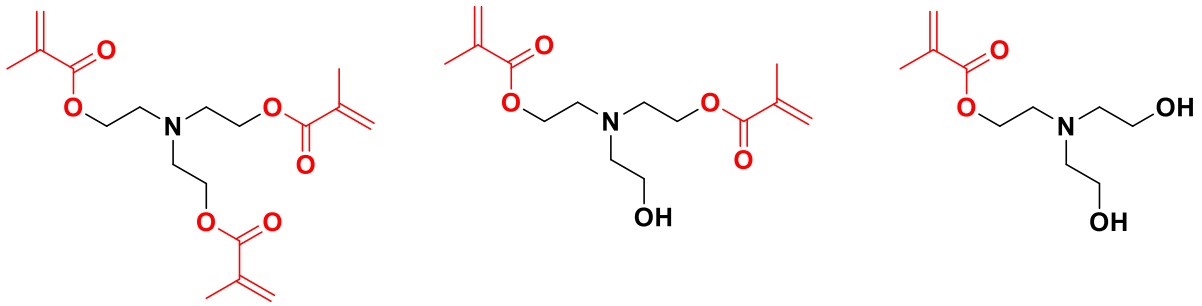

Figure 2. Final MATEOA mix composition assessed by ^{1}H-NMR in $CDCl_3$ at 293K.

Because the synthesized monomer has been utilized as a chemical building block for polymer network formations, it was strictly necessary to determine an accurate, effective molar mass for the mixture to ensure precise stoichiometric calculations. The a molar mass was calculated using a weighted distribution based on the relative abundance and

individual molar masses of each constituent (353 g/mol for Tris, 285 g/mol for Bis, and 217 g/mol for Mono). The calculation is as follows:

$$Average\ Molar\ Mass = \left(0.70 * 353\frac{g}{mol}\right) + \left(0.07 * \frac{285g}{mol}\right) + \left(0.23 * \frac{217g}{mol}\right)$$
$$= 316.96 \sim 317\ \frac{g}{mol}$$

Regarding the efficiency of the synthesis process, the esterification reaction produced overall yields of 18.64% for the initial 0.234 mol batch and 23.67% for the subsequent 0.177 mol batch. These relatively low yields were primarily attributed to the physical properties of the materials and the necessary purification steps. Specifically, significant material was lost due to the unreacted monomers and the highly viscous final product adhering to the walls of the reaction flasks and separatory funnels. Additionally, minor mass losses inevitably occurred during the gravity filtration phase and the final removal of chloroform via vacuum rotary evaporation. Despite the low mass yield, the resulting product provided the necessary structural branching and reactive acrylate groups required for the subsequent aza-Michael network formations.

4.2 Determination of Optimum Curing Temperatures

To establish the ideal thermal conditions for the network formation, the curing kinetics of the three formulations (PriMA-PG250, PriMA-PG700, and PriMA-PGM) were evaluated via differential scanning calorimetry (DSC). Dynamic scans were performed at heating rates of 2.5, 5, and 10 °C/min, monitoring the exothermic peak corresponding to the aza-Michael addition reaction. As anticipated for kinetically controlled polymerizations, the peak exothermic temperature shifted to higher values with increasing heating rates across all samples, a phenomenon attributed to the thermal lag inherent in the reaction kinetics.

To identify the optimum isothermal curing temperature (T_{opt}), the peak temperatures were plotted against the heating rates, and a linear extrapolation to a theoretical heating rate of 0 °C/min was performed.[51] The thermal profiles and corresponding extrapolation plots for each formulation are presented in Figure 3-5.

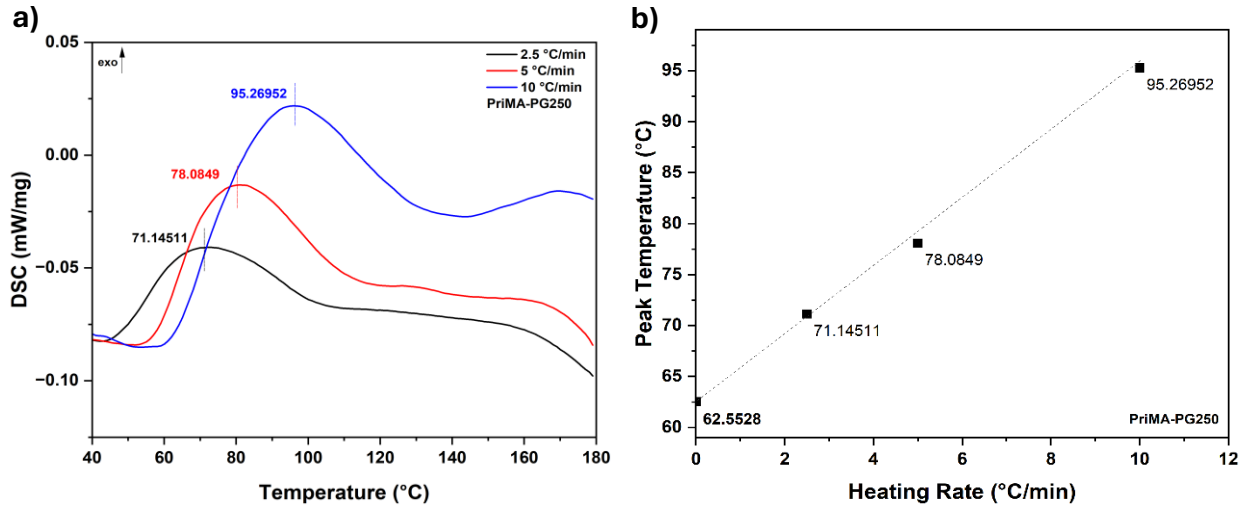

Figure 3. Determination of the optimum curing temperature for the PriMA-PG250 formulation. a) Overlaid DSC at heating rates of 2.5, 5, and 10 °C/min. b) Linear extrapolation of the peak temperatures to a 0 °C/min

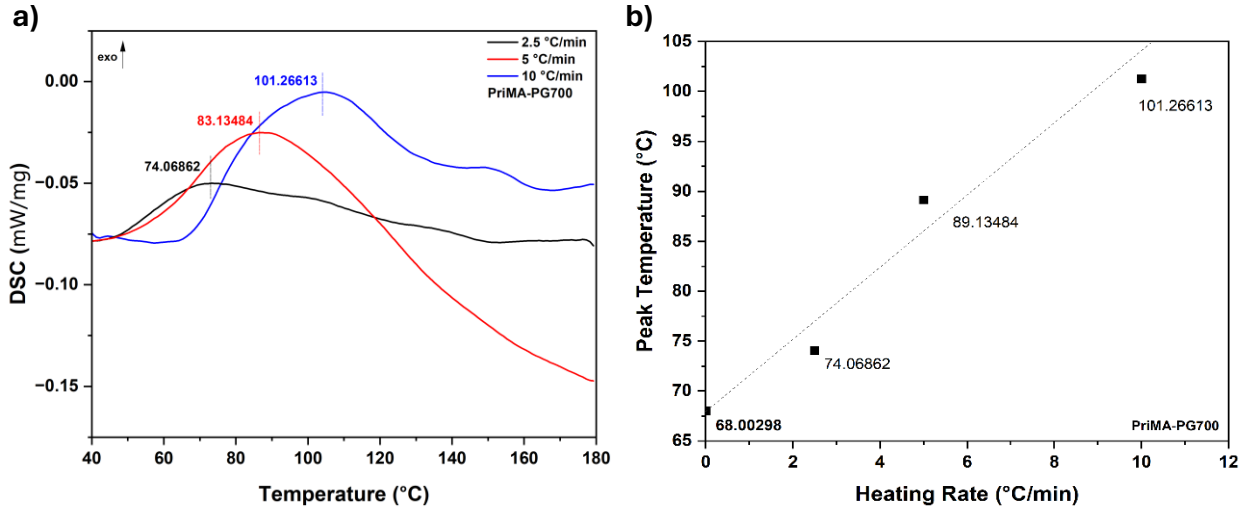

Figure 4. Determination of the optimum curing temperature for the PriMA-PG700 formulation. a) Overlaid DSC at heating rates of 2.5, 5, and 10 °C/min. b) Linear extrapolation of the peak temperatures to a 0 °C/min

The analysis revealed distinct curing requirements for each formulation. As shown in Figure 3, the PriMA-PG250 sample exhibited the lowest optimal curing temperature at approximately 63 °C. Upon increasing the molecular weight of the macromonomer in the PriMA-PG700 formulation (Figure 4), The optimum temperature rose to approximately 68 °C. This increase is attributed to the PEGDA chain effect: the longer poly (ethylene glycol) chains effectively dilute the concentration of reactive acrylate groups per unit volume. Furthermore, while longer chains generally increase flexibility, the increased distance between reactive centers likely imposes kinetic limitations, requiring higher thermal energy to efficiently initiate and sustain the crosslinking reaction.

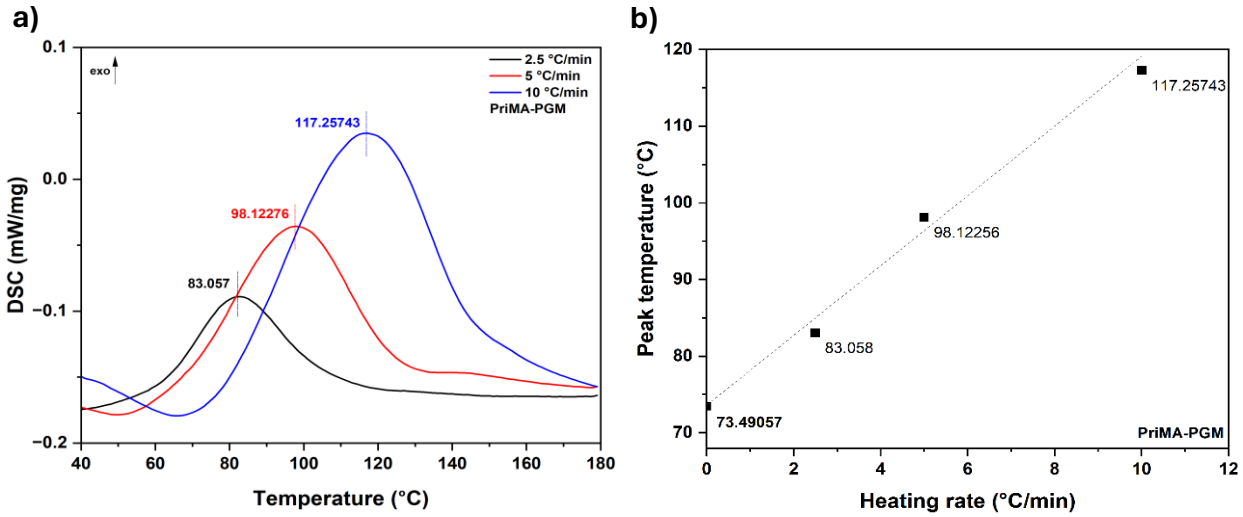

Figure 5. Determination of the optimum curing temperature for the PriMA-PGM formulation. (a) Overlaid DSC at heating rates of 2.5, 5, and 10 °C/min. (b) Linear extrapolation of the peak temperatures to a 0 °C/min

The highest optimum temperature, approximately 74 °C, was observed for the PriMA-PGM formulation, as illustrated in Figure 5. This significant increase highlights the impact of the structural hindrance introduced by the methacrylate groups. The presence of the methyl group on the double bond exerts a double inhibitory effect: electronic stabilization of the double bond (rendering it less electrophilic) and steric hindrance that physically obstructs the nucleophilic attack of the amine. Consequently, the activation energy barrier for the aza-Michael addition is raised, requiring a higher temperature to drive the reaction to completion compared to the acrylate-based analogs.

4.3 Rheological Monitoring of Network Formation

To evaluate the in-situ curing kinetics and determine the gelation point of the prepolymer resins, rheological temperature sweeps were conducted following the parallel-plate methodology detailed in the experimental section. By continuously monitoring the crossover point where the storage modulus (G') surpasses the loss modulus (G''), the liquid-to-solid transition (gel point) of each dynamic network was accurately quantified. The evolution of the module is presented in Figure 6a-c. Additionally, the time derivative of the storage modulus (dG'/dt) was plotted to evaluate the rate of network formation. The corresponding derivative curves are presented Figure 6d.

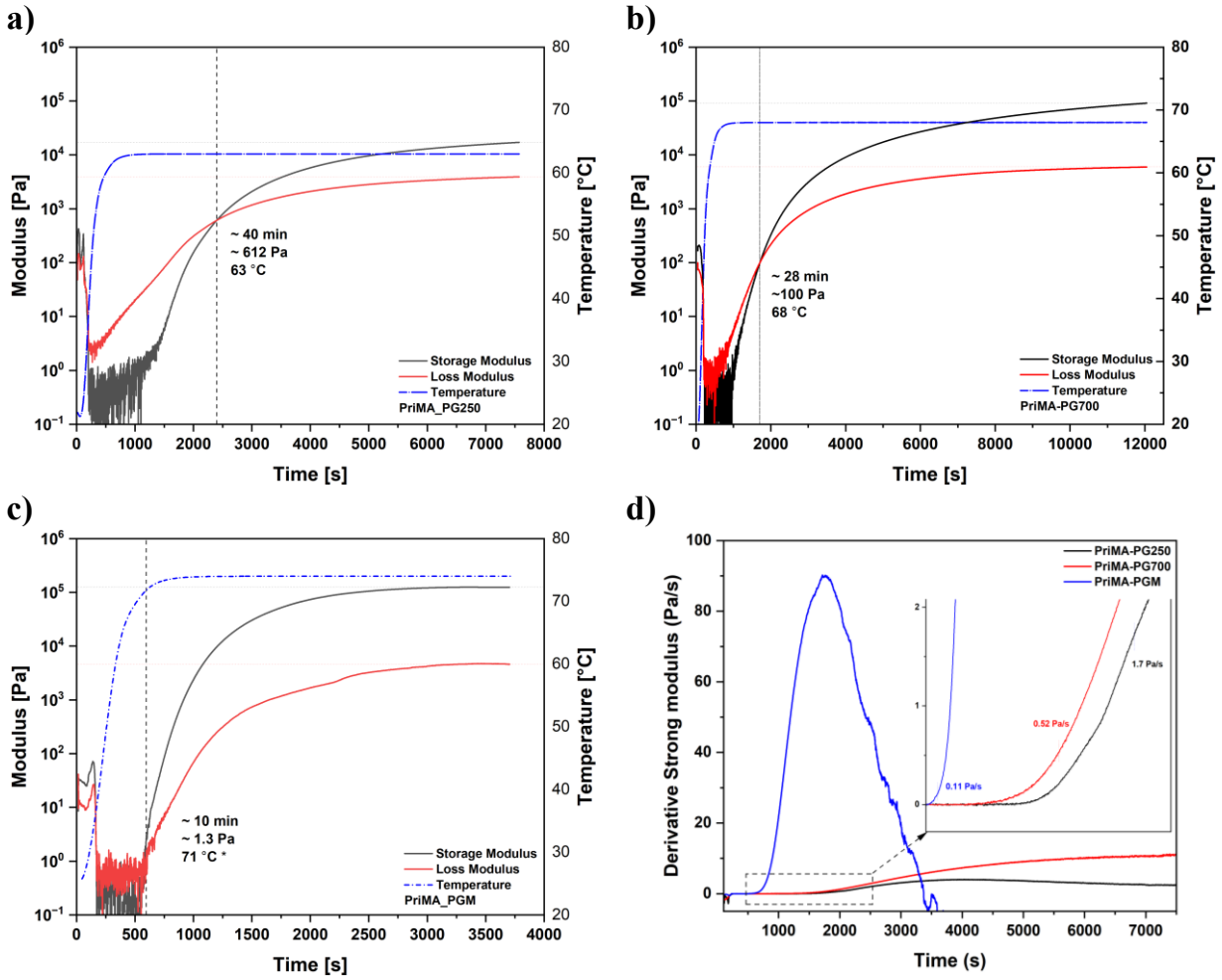

Figure 6.Rheological monitoring of the in-situ aza-Michael curing process for (a) PriMA-PG250, (b) PriMA-PG700, and (c) PriMA-PGM (d) time derivative of the storage modulus (dG'/dt)

A direct comparison of the acrylate-based formulations reveals that chain length strongly influences both the onset of gelation and the subsequent rate of structure buildup. The PriMA-PG250 network exhibited the most stable and balanced curing behavior, starting with an extended 40-minute induction time and a moderate initial structure build-up slope of 1.7 Pa/s at the gelation point. This suggests a well-ordered network formation from the onset. Post-gelation, its kinetic rate increased to a peak of ~4 Pa/s before gradually declining. This classic "rise and fall" profile indicates a highly controlled reaction that accelerates, reaches a maximum structural rate, and then naturally slows down as the network vitrifies and completes the cure.[52]

In contrast, introducing longer poly (ethylene glycol) chains in the PriMA-PG700 formulation accelerated physical gelation to approximately 28 minutes but resulted in a slow initial stiffening rate of 0.52 Pa/s at gelation point. This lower initial rate reflects the formation of a looser early network due to the highly flexible aliphatic spacer. Uniquely,

the kinetic rate for PG700 subsequently climbed to ~11 Pa/s and did not experience a drop-off during the measurement window. This sustained rate demonstrates that the longer polymer chains provide sufficient molecular mobility to prevent early vitrification, allowing the aza-Michael reaction to continue building modulus steadily without hitting a diffusion limit. This diffusion-controlled regime occurs post-vitrification when the densifying matrix physically traps unreacted functional groups, drastically dropping the overall reaction rate as these moieties can no longer physically navigate the solid network to reach one another.[53]

The most severe deviation in curing behavior, characterized by rapid initial network formation & early vitrification, was observed in the methacrylate-based PriMA-PGM formulation. This sample showed the fastest physical gelation (~10 minutes) but the weakest initial network development (0.11 Pa/s), implying that the network structurally locked before any significant mechanical strength had developed. Following this weak start, the reaction rate spiked dramatically to an extreme ~90 Pa/s. However, this massive kinetic spike was immediately followed by a sharp decline. This distinct profile confirms that the material reacts so violently and non-uniformly that it quickly vitrifies, trapping unreacted functional groups and arresting the cure prematurely.

To overcome these inherent reactivity limitations and achieve higher conversion the methacrylate aza-Michael addition, several targeted synthetic and processing strategies can be employed. Chemical modifications, such as utilizing Lewis acid catalysts to coordinate with the carbonyl oxygen[54,55] or introducing protic solvents to assist proton transfer[56], can actively enhance the polarity of the β-carbon and stabilize intermediate transition states. Alternatively, physical processing interventions like targeted microwave irradiation[57] or high-pressure processing[58] can be applied to provide localized activation energy and physically force molecular closeness, effectively bypassing the steric barriers to achieve a fully realized polymer network.

4.4 Thermal Stability and Degradation Behavior

To evaluate the thermal stability and degradation pathways of the cured networks, thermogravimetric analysis (TGA) was performed under air. The dynamic weight loss profiles and their corresponding derivative thermogravimetry (DTG) curves are presented in Figure 7a and Figure 7b, respectively. As shown in the thermograms, all three formulations exhibit a complex, multi-stage thermo-oxidative degradation process.

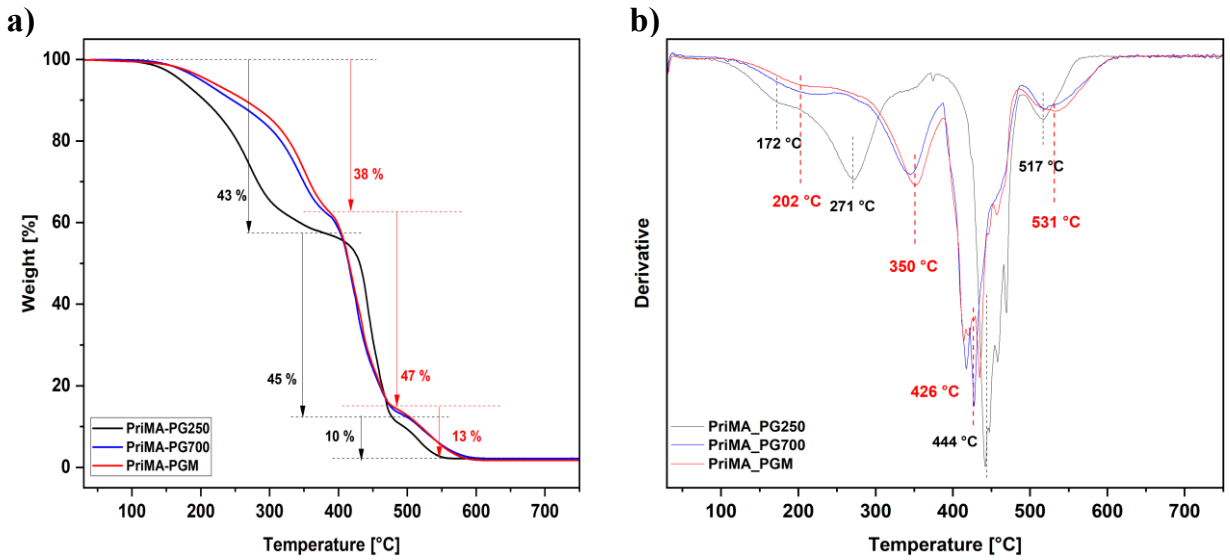

Figure 7. Thermo-oxidative degradation profiles of the synthesized networks in air: (a) TGA weight loss curves and (b) corresponding DTG derivative curves

The first degradation stage primarily involves scission of the ester and ether linkages within the polymer networks. In this initial phase, the PriMA-PG250 formulation exhibits a higher mass loss of 43%, which is a direct consequence of its higher density of highly susceptible acrylate ester bonds. Conversely, the methacrylate-based PriMA-PGM formulation displays a lower initial mass loss of 38%, reflecting the inherent thermal resistance provided by the methacrylate structure. Furthermore, the combined effect of increasing the chain length and introducing the methacrylate content elevates the first-stage onset temperature from 172 °C (for PG250) to 202 °C (for PGM), effectively extending the initial thermal stability window from 271 °C up to 350 °C.

The second major degradation stage represents the breakdown of the stable Priamine alkyl backbone (C–C bonds) and the specific aza-Michael crosslink points (C–N bonds). This is accompanied by extensive β-scission and comprehensive oxidative degradation, yielding CO_2, H_2O, and various small molecular fragments. While the overall degradation profiles remain relatively similar across all samples during this extensive mass loss phase (accounting for 45–47% of the total mass), the PriMA-PG250 network exhibits a slightly higher decomposition peak at 444 °C.

Finally, the third degradation stage involves the progressive oxidation of the residual carbonaceous residues into CO_2 and H_2O, eventually leaving behind only a trace of inorganic ash after total backbone destruction (less than 2%). In this final, high-temperature regime, the PriMA-PG700 and PriMA-PGM formulations exhibit more thermal resistance, evidenced by a distinct shift in their final degradation peak to 531 °C compared to the shorter PG250 network. This enhanced stability is directly attributed to the increased chain

length and molar mass of their respective macromolecular spacers. As established in the literature, increasing the monomer chain length and molar mass systematically delays chain scission and raises the ultimate decomposition temperature.[59]

4.5 Network Conversion and Structural Evolution by FTIR Analysis

To evaluate the curing efficiency and track the chemical evolution of the polymer networks during the aza-Michael addition, ATR-FTIR spectroscopy was performed. The conversion of the reactive monomers into the cross-linked β-amino ester network was monitored across the prepolymer, partially cured (3 hours), and fully cured (72 hours)[1,46] states for PriMA-PG250 (Figure 8a-d), PriMA-PG700 (Figure 9a-d), and PriMA-PGM (Figure 10a-d). Notably, to ensure maximum possible conversion given its hindered reactivity, the PriMA-PGM sample required one week of curing.

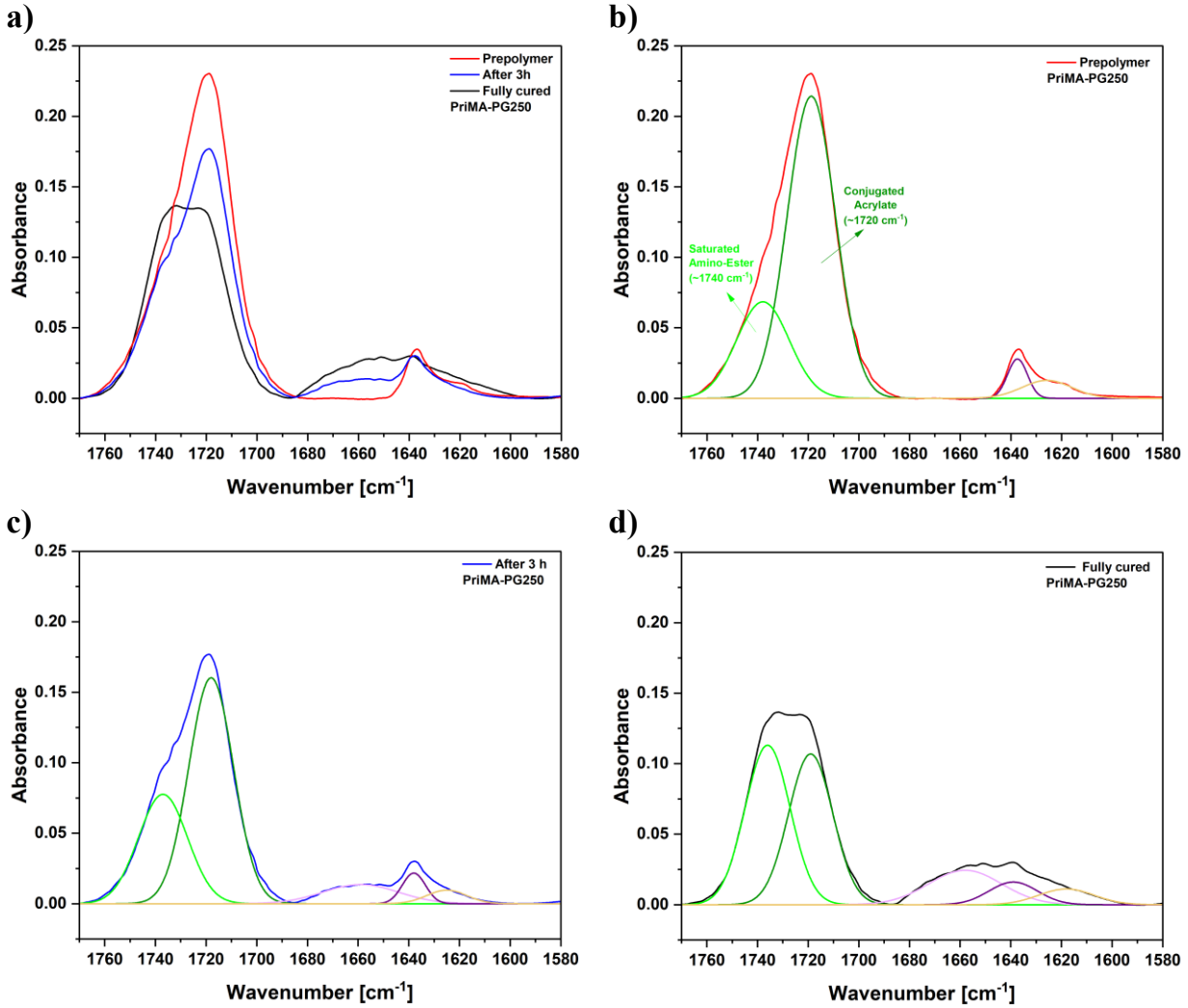

Figure 8. FTIR spectra comparison of (a) the baseline PriMA-PG250 formulation, (b) at prepolymer, (c) partially cured (3h), and (d) fully cured (72h) states

As shown in Figure 8a-d, the baseline network demonstrates a clear emergence of the saturated ester peak at ~1740 cm^{-1}, indicating successful, robust network formation. However, the conjugated peak at 1720 cm^{-1} does not fully disappear, pointing to a balanced but incomplete conversion where some functional groups are eventually trapped as the tighter network gels. To mathematically validate this, Gaussian fitting reveals that the area ratio of the saturated carbonyl to the conjugated carbonyl (A_{1740} / A_{1720}) increased from 0.34 in the prepolymer state to a balanced 1.07 in the fully cured state.

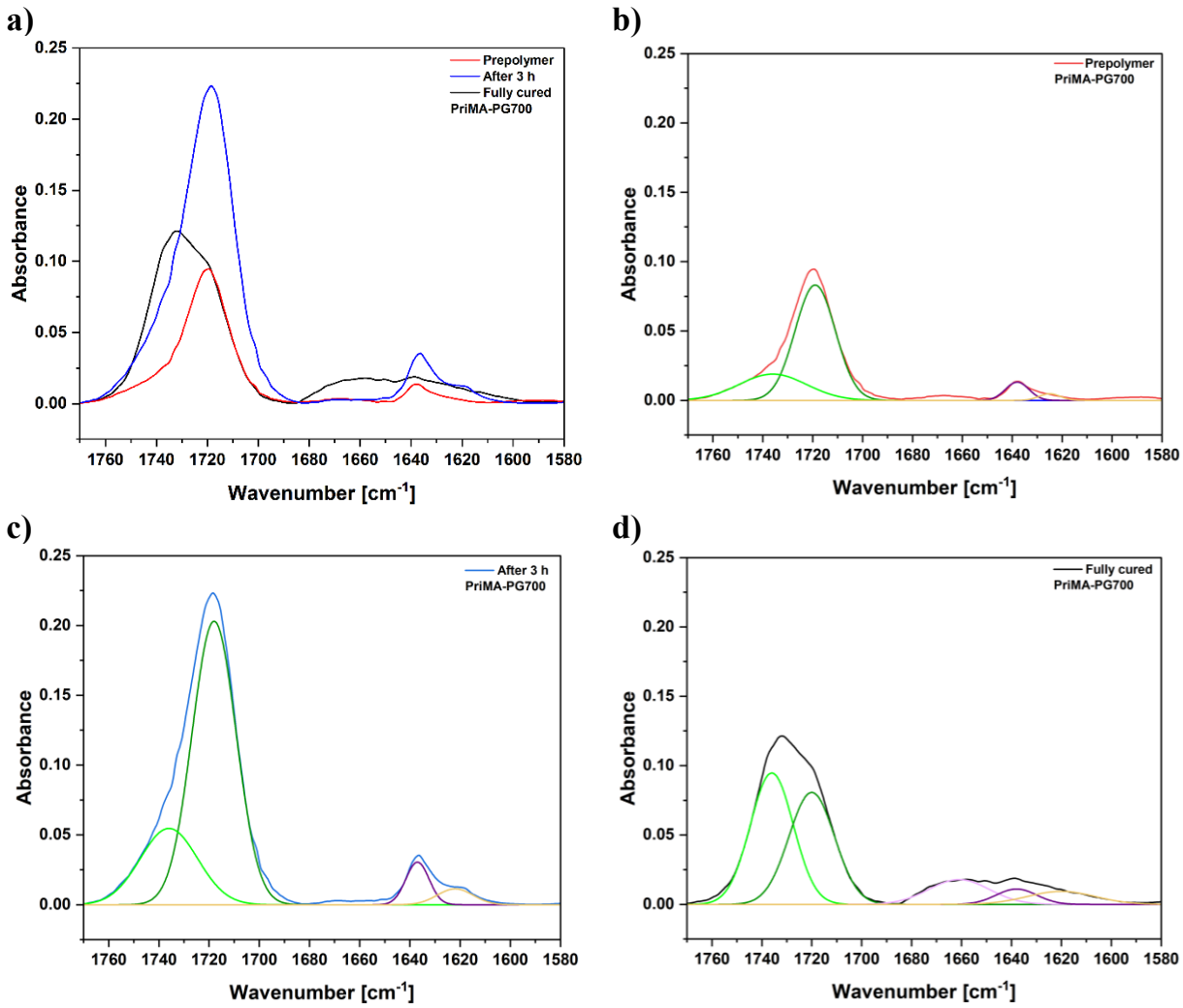

Figure 9. FTIR spectra comparison of (a) the baseline PriMA-PG700 formulation, (b) at prepolymer, (c) partially cured (3h), and (d) fully cured (72h) states

The PriMA-PG700 formulation (Figure 9a-d) exhibits the most dramatic spectral shift. In the fully cured state, the saturated amino-ester peak (~1740 cm^{-1}) overtakes the original conjugated peak, becoming the dominant feature in the carbonyl region. This confirms that the longer, flexible PEG700 chains provide sufficient molecular mobility, allowing the reactive groups to maintain contact and react extensively. This high degree of conversion

is supported by the quantitative area ratio (A_{1740} / A_{1720}), which surged from 0.38 in the prepolymer to a dominant 1.10 after full curing.

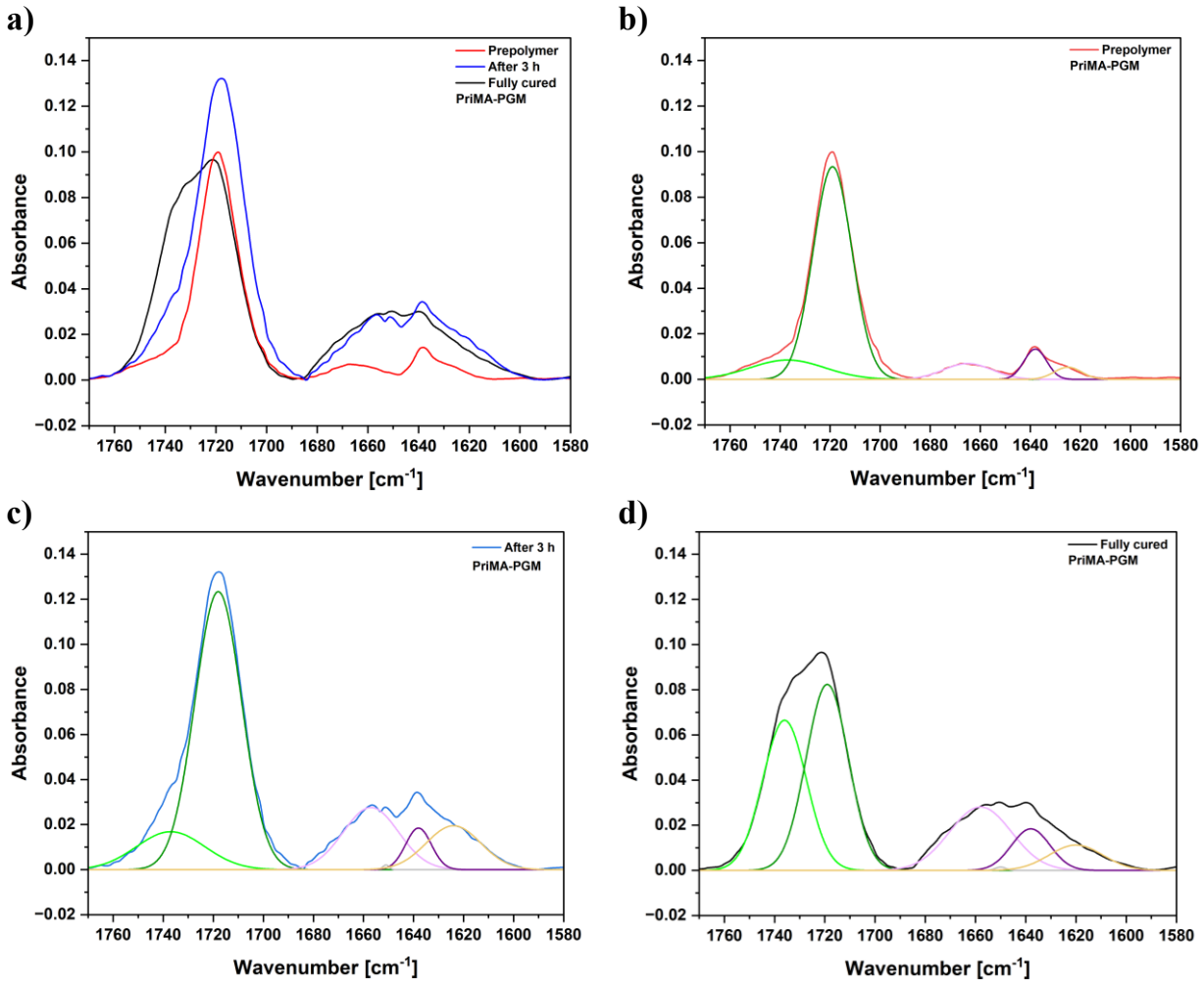

Figure 10. FTIR spectra comparison of (a) the baseline PriMA-PGM formulation, (b) at prepolymer, (c) partially cured (3h), and (d) fully cured (72h) states

In contrast, the PGM formulation (Figure 10a-d) retains the conjugated peak (~1720 cm^{-1}) as its dominant feature even after the full week curing cycle, with the saturated ester appearing merely as a smaller shoulder. This validates the rheological data: the bulky, electron-donating methyl groups of the methacrylate heavily restrict reactivity through steric hindrance, leading to premature physical "locking" of the network (vitrification) before substantial chemical conversion can occur. Quantitative analysis confirms this minimal progression, with the area ratio (A_{1740} / A_{1720}) increasing from 0.17 in the prepolymer to only 0.83 in the fully cured state, completely failing to invert the peak dominance.

Across all three formulations (PriMA-PG250, PriMA-PG700, and PriMA-PGM), FTIR analysis of the fully cured samples revealed consistent evidence of a universal competitive side reaction. Specifically, a broad absorption band emerged post-cure in the 1640–1680 cm^{-1} region, which is uniquely characteristic of amide I vibrations.[60] This indicates that rather than exclusively undergoing the target aza-Michael addition at the β-carbon, a fraction of the primary amines directly attacked the ester carbonyls to form amide linkages. Because this competitive pathway occurs across all tested systems, it demonstrates that this side reaction is an inherent feature of these mixed amine-ester chemistries, consuming reactive equivalents.[61]

4.6 Thermomechanical Properties and Crosslinking Density

The solid-state viscoelastic properties and thermomechanical behavior of the successfully cured networks were evaluated using dynamic mechanical analysis (DMA) in tensile mode, following the thermal and geometric parameters detailed in the experimental section. Because the PriMA-PGM formulation suffered from early vitrification and severe incomplete curing, it could not form an isolated, structurally sound solid specimen and was therefore excluded from this specific analysis. The thermomechanical profiles for the viable PriMA-PG250 and PriMA-PG700 networks are presented in Figure 11.

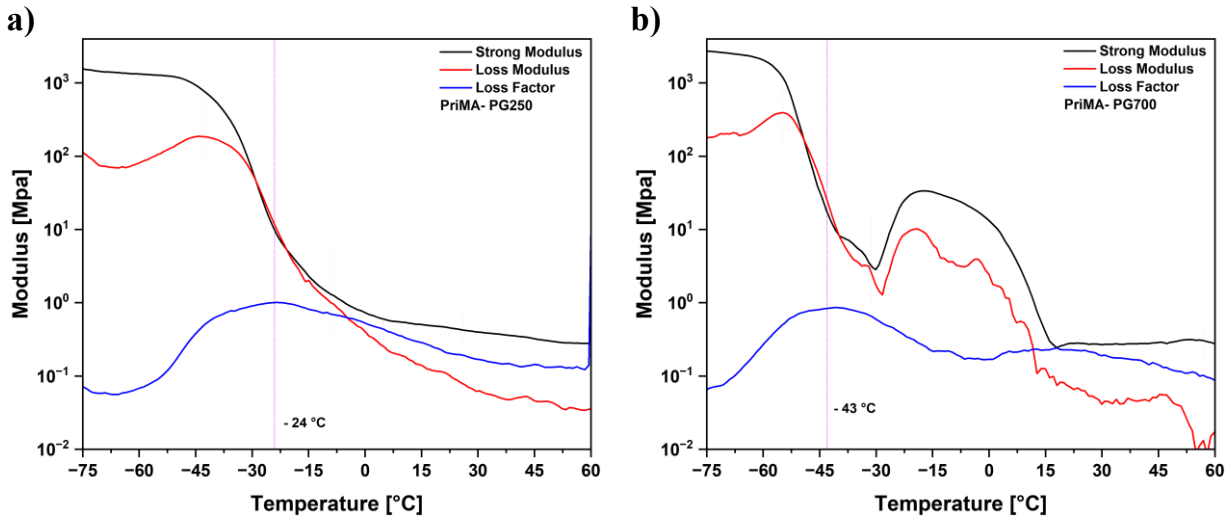

Figure 11. DMA thermomechanical profiles detailing the evolution of storage modulus (E'), loss modulus (E''), and tan δ for (a) the PriMA-PG250 network and (b) the PriMA-PG700 network

In accordance with the theory of rubber elasticity[62], the primary thermal transition for each network was identified as the α-transition temperature (T_α), which was determined from the maximum peak of the respective tan δ curve. The measured T_α demonstrated a strong dependence on the length of the macromolecular crosslinker segment. The baseline PriMA-PG250 network exhibited a T_α of -24 °C alongside an initial onset of storage modulus (E') decrease at approximately -35 °C. In contrast, incorporating the longer chains in the

PriMA-PG700 formulation shifted the T_α significantly lower to -43 °C, with the modulus drop beginning much earlier at -56 °C. This substantial difference confirms that the longer, highly flexible poly (ethylene glycol) segments increase the free volume and molecular mobility within the matrix, yielding a more rubbery network at lower temperatures.

It is important to emphasize that because DMA is a dynamic measurement applying a continuous physical frequency, the resulting molecular lag inherently shifts the measured T_α approximately 10 to 20 °C higher than the absolute thermodynamic glass transition temperature T_g.[63] Consequently, quasi-static differential scanning calorimetry (DSC) measurements will be presented in the subsequent section to definitively confirm the thermodynamic T_g of the formulations.

Furthermore, the thermomechanical profile of the PriMA-PG700 formulation displayed a broadened transition region with secondary modulus fluctuations. This behavior is attributed to strain-induced crystallization, a phenomenon where the cyclic loading applied during the test physically aligns the longer, flexible PEG chains into localized crystalline domains.[64]

To quantitatively evaluate network connectivity, the apparent crosslinking density was calculated using the method described in the experimental section. For the standard PriMA-PG250 network, E' was registered at the conventional $T = T_\alpha + 100$ °C (76 °C), yielding a modulus of 0.42 MPa and a corresponding crosslinking density of 56.5 mol/m^3. However, to ensure the measurement for PriMA-PG700 was taken completely outside the anomalous region affected by the suspected strain-induced crystallization, E' was deliberately evaluated further along the plateau at $T = T_\alpha + 100$ °C (57 °C). At this elevated temperature, the PG700 network exhibited a rubbery modulus of 0.306 MPa, resulting in a crosslinking density of 37.17 mol/m^3. While this quantitative reduction mathematically confirms that the extended PEG700 chains create a significantly looser macroscopic architecture, it is also crucial to note the physical state of the specimens. Due to the high reactivity of the amine-acrylate couple (mostly coming from Priamine1071), visible bubbles were observed remaining within the cured thermosets. As documented in the literature, such trapped gaseous inclusions can act as macroscopic defects, directly contributing to a reduction in the bulk thermo-mechanical properties (such as the observed E' plateau values) across the samples.[46]

4.7 Glass Transition and Crystallinity by DSC Analysis

The thermal behavior of all the formulations was investigated using Differential Scanning Calorimetry (DSC), with the resulting thermograms for PriMA-PG250, PriMA-PGM, and PriMA-PG700 presented in Figure 12a-c. These plots reveal distinct differences in the

ability of each formulation to organize into crystalline structures, which is heavily dictated by its specific molecular architecture.

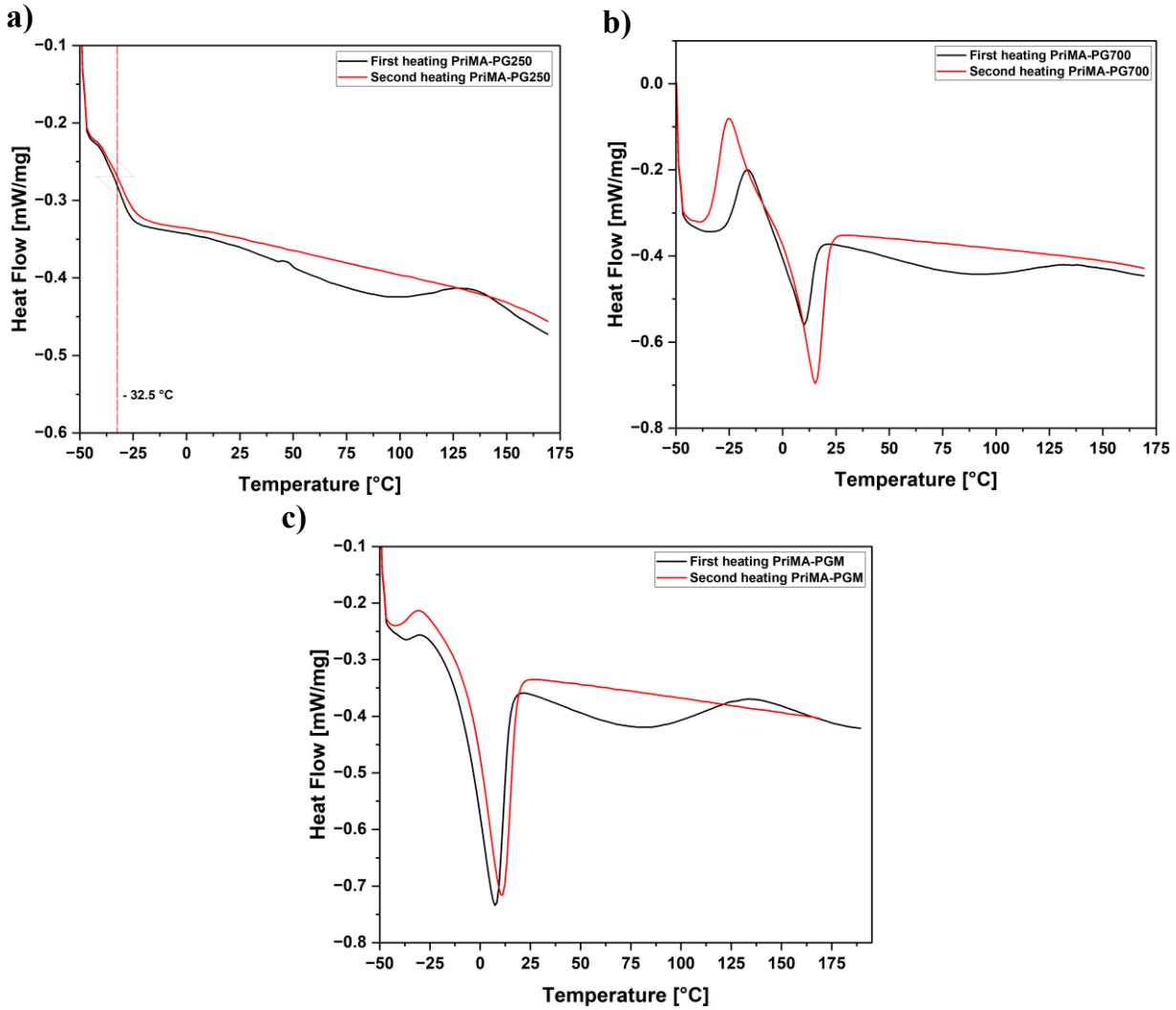

Figure 12. DSC thermograms of the first and second heating cycles for (a) PriMA-PG250, (b) PriMA-PG700, and (c) PriMA-PGM

The thermograms show significant differences between the first and second heating cycles due to the material's initial thermal history. Heating through the first scan and cooling at a controlled rate erases prior processing variations, establishing a reproducible thermal history for accurate comparison.

For the PriMA-PG250 formulation (Figure 12a) the glass transition temperature (T_g) is clearly visible as a characteristic step-change in heat capacity, determined to be -32.5 ˚C. Notably, this static value perfectly corroborates the dynamic mechanical data discussed previously, displaying the anticipated theoretical offset from the dynamically measured T_α (-24 °C). Furthermore, this sample exhibits no endothermic or exothermic peaks

throughout the heating cycle. This absence indicates a predominantly amorphous structural network where the polymer chains lack the necessary length, symmetry, or mobility to undergo crystallization under the tested conditions.

The distinctly lower T_g of -32.5 °C for PriMA-PG250 highlights the chain mobility and free volume granted by the flexible PEGDA-250 and Priamine combination. This aligns perfectly with previous studies demonstrating that PEGDA-based networks inherently exhibit low T_g values (typically ranging from −40 to −30 °C).[64] While the soft aliphatic chains of Priamine generally promote flexibility, literature shows that other Priamine-based thermosets can still reach higher T_g values (e.g., 13 °C) when driven by exceptionally high conversion and tight cross-linking density.[46] The T_g of -32.5 °C observed in the PriMA-PG250 network therefore confirms that the PEGDA-250 increases the network's free volume.

In contrast to the fully amorphous behavior of PG250, the PriMA-PGM and PriMA-PG700 formulations (Figure 12b and Figure 12c) exhibit complex phase transitions indicative of semicrystalline materials. For these formulations, endothermic melting peaks are observed in the ranges of -15 to 20 °C and -5 to 25 °C, respectively. Immediately preceding these melting endotherms, pronounced exothermic peaks are observed. These exothermic events are attributed to cold crystallization, a characteristic feature of crystalline polymers that retain a high degree of amorphous phase following rapid cooling.[65]

The mechanism behind this phenomenon is intrinsically linked to the thermal energy and segmental mobility of the polymer. During the cooling process, the rapid drop in temperature effectively freezes the polymer chains in a disordered, glassy state before they have adequate time to arrange into a crystalline lattice.[66] Upon reheating, once the material passes its T_g and transitions from a rigid glassy state to a rubbery state, the polymer chains gain sufficient micro-Brownian mobility to reorganize themselves into an ordered crystalline structure.[67] This crystallization process releases latent heat, which is recorded as the exothermic peak in the DSC thermogram. Crucially, while cold crystallization is kinetically triggered by the onset of chain mobility at the glass transition, the precise T_g step-change is not visible in the PG700 and PGM thermograms. Based on the dynamic mechanical analysis (which recorded a T_α of -43 °C for the PG700 network), the static thermodynamic T_g is theoretically expected to be 10 to 20 °C lower. Therefore, it is highly probable that the true T_g of these highly flexible formulations falls below the -50 °C lower limit of the DSC heating program, meaning the characteristic baseline shift occurs just before the data acquisition window.

4.8 Gel Content

To quantitatively assess the structural integrity and curing efficiency, gel content measurements were conducted via solvent extraction in chloroform, following the ASTM standard methodology detailed in the experimental section. A summary of the gel fraction data is presented in Table 2.

Table 2. Summary of gel content results obtained via chloroform solvent extraction

Samples	Initial weight (mg)	Final weight (mg)	Gel content (%)
PriMA-PG250	37.7	31.7	**84.1**
PriMA-PG700	81.2	45.3	**55.8**
PriMA-PGM	45.7	14.3	**31.3**

A direct comparison of the formulations reveals stark differences in their ultimate structural development. The PriMA-PG250 formulation yielded a high gel content of 84.1%, indicating the successful formation of a highly interconnected and mainly insoluble network. This robust connectivity perfectly correlates with its controlled curing profile observed during rheological testing. Balanced structural buildup allowed the reactive monomers sufficient mobility and time to be nearly entirely incorporated into the infinite gel architecture before vitrification.

In contrast, incorporating extended poly (ethylene glycol) chains into the PriMA-PG700 formulation resulted in a moderate gel content of 55.8%. This moderate structural connectivity contrasts with the highly efficient chemical conversion previously confirmed by FTIR analysis. This difference indicates a distinct structural trade-off; while the local functional groups possessed sufficient mobility to react extensively, the highly flexible, elongated chains largely formed a looser, less dense macroscopic network. Consequently, a significant portion of the reacted material likely formed soluble extractables (sol fraction) or intramolecular loops (primary cyclization)[68,69] that do not actively contribute to the load-bearing, infinite gel structure.

The most critical deviation was observed in the methacrylate-based PriMA-PGM formulation, which exhibited a low gel content of 31.3%, and nearly 70% of the resulting material remains entirely soluble, consisting primarily of unreacted monomers and low-molecular-weight oligomers. This severely low value provides definitive physical evidence supporting the premature vitrification hypothesis. Driven by the extreme steric hindrance of the methacrylate groups, the network physically "locked up" well before the chemical

conversion could be completed, leaving behind a highly defective, weak, and largely extractable structure.

4.9 Stress relaxation analysis

4.9.1 Macroscopic Relaxation Dynamics and Activation Energy

To evaluate the dynamic bond exchange kinetics and the macroscopic viscoelastic flow of the synthesized vitrimer networks, isothermal stress-relaxation profiles were analyzed. The evolution of the normalized relaxation modulus, $G(t)/G_0$, was continuously monitored over a logarithmic time scale at various elevated temperatures (Figure 13). To quantitatively determine the activation energy (E_a) of the dynamic transesterification process, characteristic relaxation times were extracted and analyzed using two distinct analytical approaches based on the Arrhenius temperature dependence.[70]

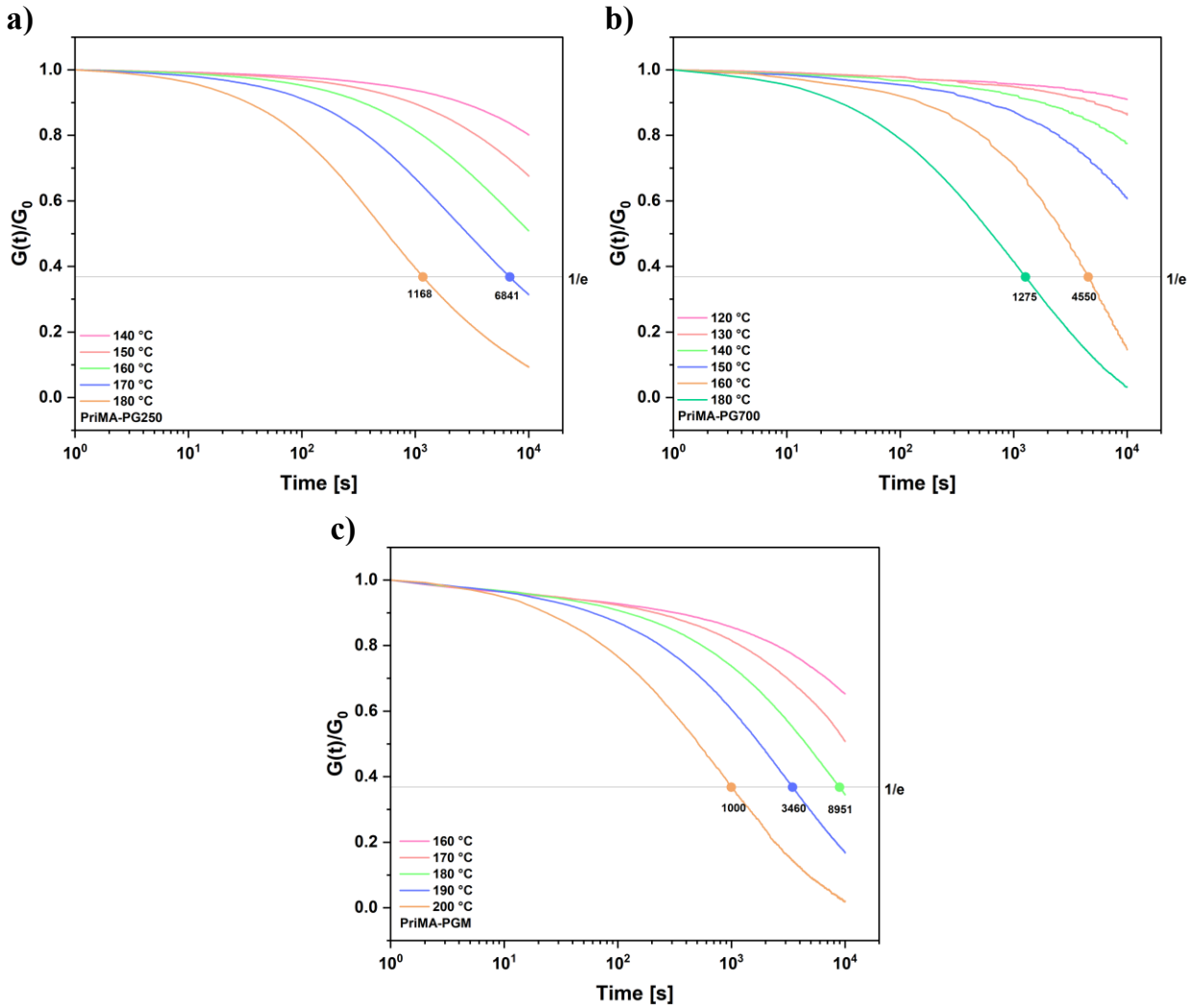

Figure 13. stress-relaxation profiles (left column) for (a) PriMA-PG250, (b) PriMA-PG700, and (c) PriMA-PGM and corresponding master curves (Right Column)

The first method directly evaluates the individual isothermal curves by defining the terminal relaxation time (τ) as the specific point where the normalized relaxation modulus decays to 1/e (approximately 36.8%) of its initial value.[71] These specific characteristic points are visually denoted on the unshifted relaxation curves for each formulation (Figure 13a-c). Because the macroscopic relaxation is governed by the thermally activated bond exchange, the natural logarithm of these extracted relaxation times, ln(τ), exhibits a linear dependence on the inverse absolute temperature (1000/T) according to the Arrhenius equation:[70,72]

$$\ln(\tau) = \ln(\tau_0) + \frac{E_a}{RT}$$

where τ_0 is the pre-exponential factor, and R is the universal gas constant (8.314 $J \cdot K^{-1} \cdot mol^{-1}$). By plotting ln(τ) versus 1000/T, a linear fit is generated. The activation energy is then directly calculated by extracting the slope of this line (E_a/R) and multiplying it by R.

The second approach utilized the Time-Temperature Superposition (TTS) principle to account for the broader viscoelastic response across an extended timescale.[73] Master curves were constructed by shifting each isothermal relaxation curve horizontally along the logarithmic time axis relative to a chosen reference temperature (Figure 14a-c). This physical transformation maps the experimental time to an effective time, yielding the empirical time shift constant (a_T).[74] Because the accelerated relaxation at higher temperatures is driven by the same dynamic exchange mechanism, the shift factors also follow an Arrhenius relationship: [73,75]

$$\ln(a_T) = \frac{E_a}{R}\left(\frac{1}{T} - \frac{1}{T_{ref}}\right)$$

Similar to the first method, plotting the shift factors ($\ln(a_T)$) against the inverse temperature (1000/T) produces a linear slope. Extracting this slope (E_a/R) and multiplying it by the gas constant provides a secondary, independent calculation of the activation energy that evaluates the entire relaxation profile rather than a single terminal decay point.

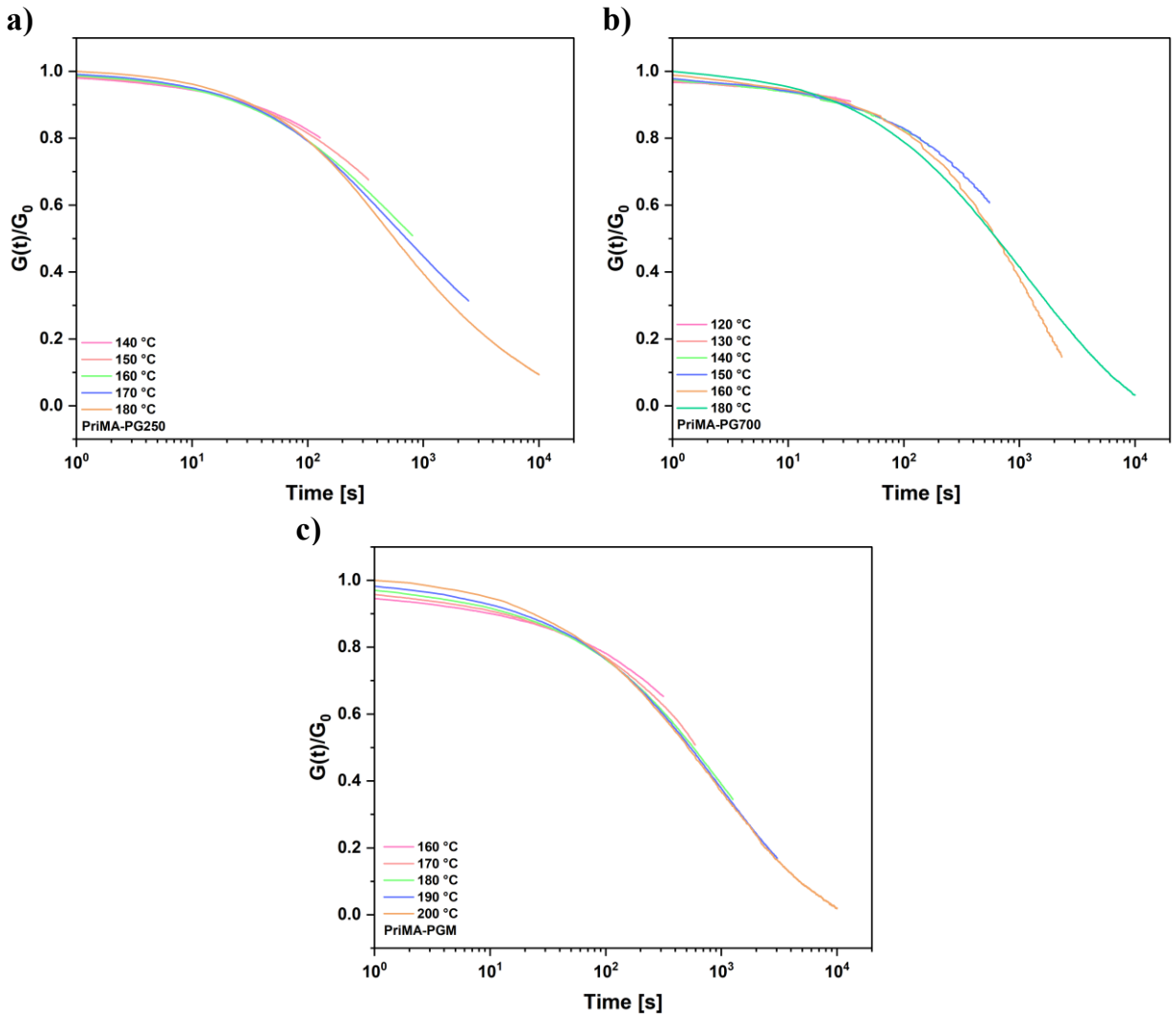

Figure 14. stress-relaxation profiles constructed by shifting the isothermal data along the time axis for (a) PriMA-PG250, (b) PriMA-PG700, and (c)

The corresponding Arrhenius plots, demonstrating the linear dependence of $\ln(\tau)$ and $\ln(a_T)$ on the inverse absolute temperature, are presented in Figure 15. A comprehensive summary of the extracted E_a values for all three formulations is provided in Table 3.

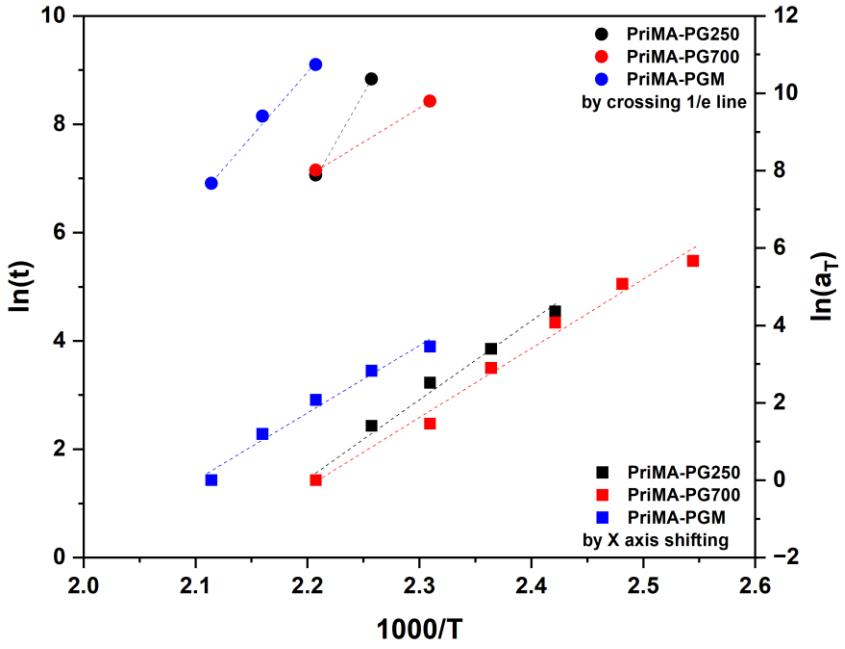

Figure 15. Linear fits of characteristic relaxation times (ln(τ)) and TTS shift factors (ln(a_T)) against 1000/T for E_a determination

Table 3. Summary of the activation energies (E_a) for the dynamic bond exchange

Formulation	*E_a from 1/e decay (kJ/mol)*	*E_a from TTS shifting (kJ/mol)*
PriMA-PG250	294.9	166.2
PriMA-PG700	103.7	148
PriMA-PGM	195	145

Topological architecture directly dictates the activation energy of the dynamic exchange. When compared to the literature, typical transesterification-type vitrimers, including various epoxy-based networks, generally exhibit E_a values between 70 and 160 kJ/mol.[75–77] The structurally flexible PriMA-PG700 formulation falls perfectly within this standard range with an E_a of 103.7 kJ/mol (derived from terminal relaxation), demonstrating a high rate of dynamic exchange characteristic of highly mobile networks. Conversely, the prematurely vitrified PriMA-PGM (E_a = 195.0 kJ/mol) and the robustly cross-linked PriMA-PG250 (E_a = 294.9 kJ/mol) exhibit terminal activation energies well above this typical threshold. While less common, similarly high activation energies (ranging from 160 to 250 kJ/mol) have been reported in specific high-performance systems, where they are shown to heavily favor the creation of dynamic elastomers with outstanding creep resistance at elevated service temperatures.[1,75] Furthermore, recent literature emphasizes that to successfully function as direct replacements for traditional thermoplastics, vitrimers

must undergo a massive viscosity drop between service and processing temperatures; mathematically, this requires achieving an E_a strictly greater than 200 kJ/mol[75], a demanding theoretical threshold that the densely entangled PEGDA-250 network successfully surpasses.

It is crucial to address the discrepancy observed between the E_a values calculated via the 1/e terminal decay method versus time-temperature superposition (TTS) shifting. While investigating the terminal relaxation (1/e) grants direct access to quantifying the macroscopic flow activation energy, TTS analysis incorporates the shifting of the entire relaxation spectrum. The observed deviations between the two methods confirm that the distinct structural relaxation modes within these networks (e.g., the fast mobile segments versus the heavily entangled slow tail) possess uniquely varying thermal dependencies.[71]

Furthermore, E_a dictates the temperature sensitivity of the network's macroscopic viscosity, represented by the slope of the Arrhenius curves (Figure 15). High E_a values, such as that of the densely cross-linked PriMA-PG250, indicate a rapid decrease in viscosity upon heating. This steep thermal dependence ensures robust structural stability at operating temperatures while rapidly accelerating the internally catalyzed dynamic bond exchange upon heating, ultimately enabling highly efficient thermal processing and reprocessability.[72]

4.9.2 Viscoelastic Modeling

While the activation energy (E_a) provides macroscopic insight into the dynamic bond exchange, stress relaxation in complex, highly entangled polymer networks rarely follows an ideal, monoexponential Maxwell behavior. To capture the broad distribution of relaxation times, experimental data are often initially modeled using a stretched exponential (Kohlrausch-Williams-Watts) decay: [71,78]

$$G(t) = G_0 * \exp\left(-\frac{t}{\tau}\right)^{\beta}$$

where β is a stretching parameter between 0 and 1. While this model effectively indicates a continuous, broad distribution of relaxation times, relying on a single stretching parameter limits the ability to distinctly separate the physical phases of the material, particularly when the network exhibits both a rapid early-stage relaxation and a highly extended, slow relaxation tail.[71] The corresponding KWW fitting on experimental stress relaxation presented in Figure 16a-c.

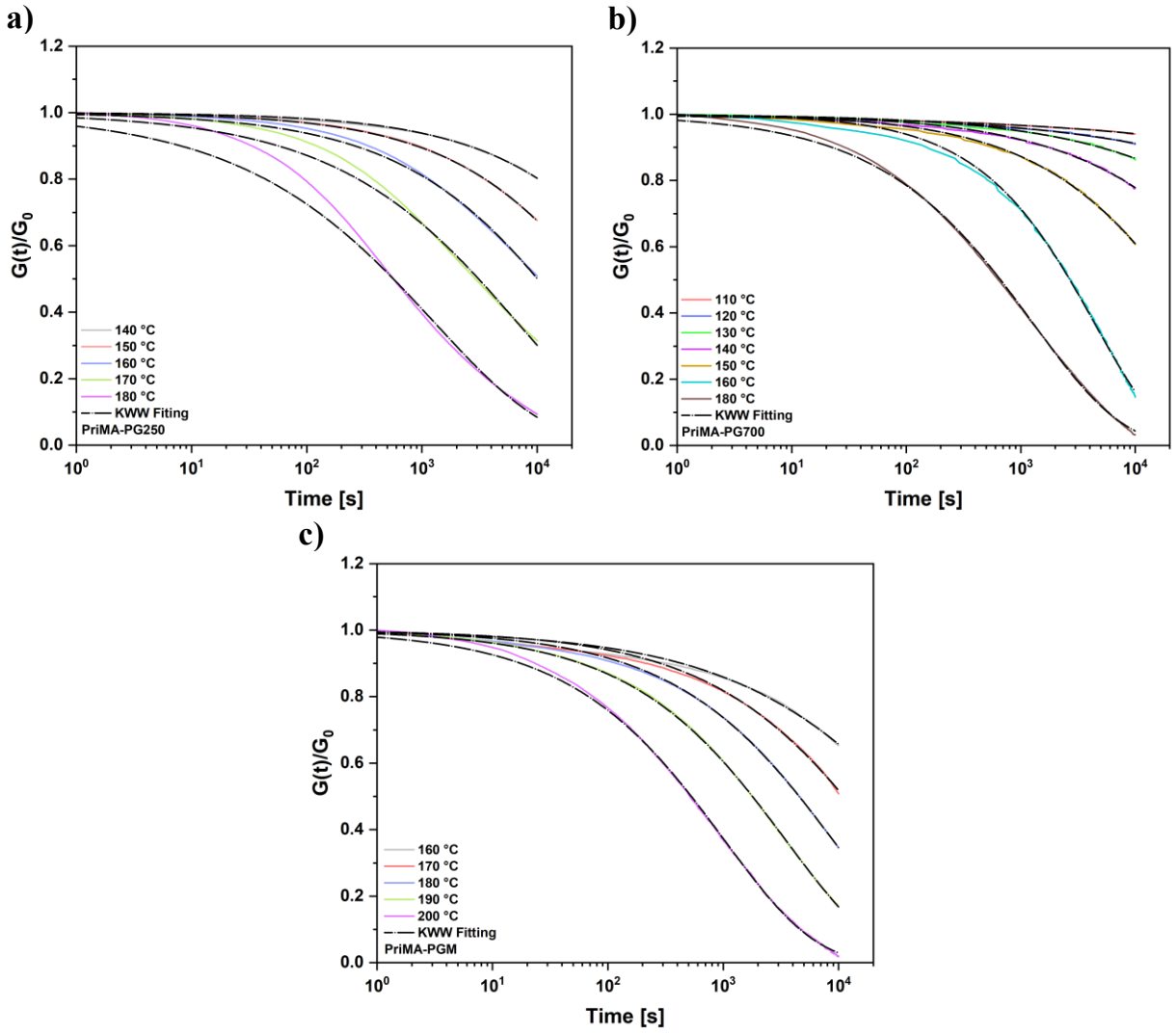

Figure 16. KWW fitting experimental stress relaxation for (a) PriMA-PG250, (b) PriMA-PG700, and (c) PriMA-PGM

To precisely resolve the discrete relaxation spectrum of the synthesized vitrimers, the stress-relaxation data were instead fitted using a Generalized Maxwell Model, mathematically expressed as a multi-term Prony series. The general equation for this discrete relaxation spectrum decomposes the macroscopic relaxation into a sum of N independent exponential decays alongside an equilibrium modulus: [75]

$$G(t) = \sum_{i=1}^{N} G_i e^{-\frac{t}{\tau_i}} + G_\infty$$

where G_i and τ_i represent the respective modulus fraction and relaxation time of the i-th Maxwell element, and G_∞ is the persistent equilibrium modulus at infinite time.

The experimental data for these specific formulations exhibited complex, multi-modal physical behaviors at elevated temperatures, beginning with an exceptionally fast initial stress drop followed by a highly entangled, slow relaxation tail. To accurately capture this entire breadth without the standard "intercept gap" caused by unconstrained least-squares fitting algorithms, a four-term Prony series (N=4) was specifically employed:

$$G(t) = G_0 e^{-\frac{t}{\tau_0}} + G_1 e^{-\frac{t}{\tau_1}} + G_2 e^{-\frac{t}{\tau_2}} + G_3 e^{-\frac{t}{\tau_3}} + G_{inf}$$

Because the experimental data represent a normalized modulus ($G(t)/G_{t=0}$), the initial value must physically equal exactly 1. Therefore, a mathematical boundary condition was applied to the fitting algorithm, strictly constraining the sum of the modulus fractions to unity ($G_0 + G_1 + G_2 + G_3 + G_\infty = 1$).

In this refined discrete model, the addition of the ultra-fast initial term (τ_0) captures the immediate relaxation of highly mobile, unentangled short segments that typical three-term models miss. The subsequent time constants (τ_1, τ_2, τ_3) represent the distinct fast, intermediate, and slow segmental dynamics of the broader network. The pre-exponential coefficients (G_0 through G_3) denote the relative weighting, effectively quantifying the percentage of the material's structural integrity governed by each specific timescale. Finally, a G_∞ indicates the presence of a persistent, solid-like network fraction that resists complete viscous flow even at elevated temperatures, providing critical insight into the ultimate topological stability of the thermoset.[75]

The experimental stress-relaxation curves, alongside their corresponding 4-term Prony series mathematical fits, are visually presented in Figure 17a–c.

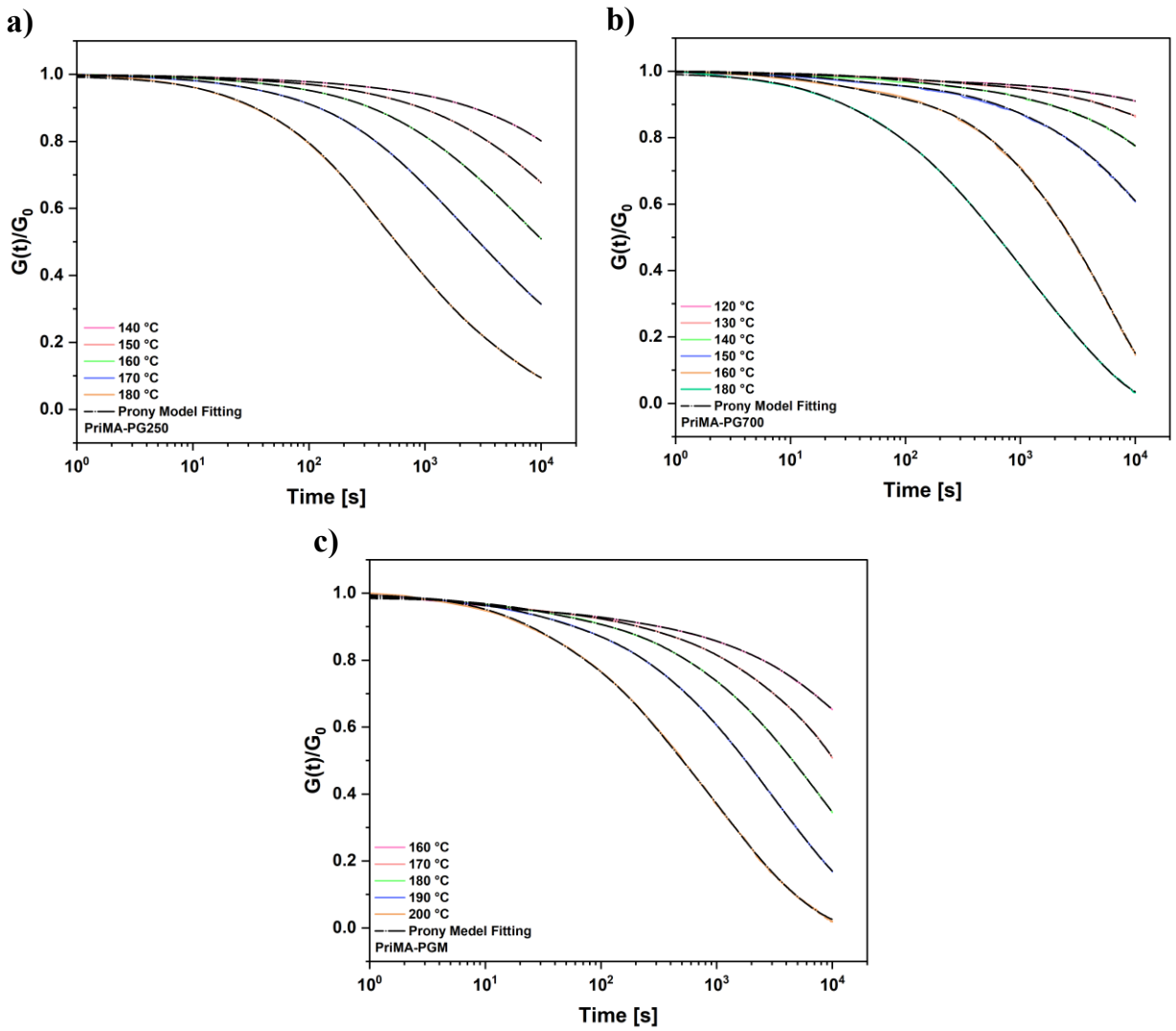

Figure 17. 4-term Prony series fits (dashed lines, $R^2 > 0.9995$) applied to the isothermal stress-relaxation data (solid lines) of (a) PriMA-PG250, (b) PriMA-PG700, and (c) PriMA-PGM.

To quantitatively assess the internal structural dynamics of the synthesized vitrimers, the extracted parameters from this Generalized Maxwell model were comprehensively analyzed for each formulation (Table 4, Table 5, and Table 6). By evaluating the evolution of the discrete modulus fractions (G_i) and the equilibrium modulus (G_∞) as a function of temperature, distinct trends regarding the topological integrity and the thermally activated disentanglement of the respective networks emerge.

Table 4. Discrete relaxation spectrum parameters for PriMA-PG250 derived from the 4-term Prony series fitting

Temp (°C)	G_0	τ_0 (s)	G_1	τ_1 (s)	G_2	τ_2 (s)	G_3	τ_3 (s)	G_∞
140	0.009	14.3	0.017	167.8	0.033	1381.4	0.284	15014.9	0.656
150	0.012	15.8	0.022	196.1	0.067	1309.6	0.352	10151.0	0.545
160	0.017	25.5	0.038	253.4	0.134	1166.4	0.407	7542.5	0.401
170	0.026	24.7	0.089	243.1	0.232	966.0	0.406	5738.6	0.243
180	0.050	25.3	0.257	186.6	0.335	797.5	0.299	4906.5	0.055

Table 5. Discrete relaxation spectrum parameters for PriMA-PG700 derived from the 4-term Prony series fitting

Temp (°C)	G_0	τ_0 (s)	G_1	τ_1 (s)	G_2	τ_2 (s)	G_3	τ_3 (s)	G_∞
120	0.009	6.1	0.020	104.1	0.012	1301.6	0.103	16040.5	0.855
130	0.011	6.6	0.020	131.0	0.013	731.4	0.152	10551.9	0.806
140	0.020	7.0	0.030	94.2	0.040	1008.9	0.317	15406.1	0.610
150	0.031	22.3	0.024	411.6	0.045	931.2	0.438	9199.0	0.462
160	0.053	25.0	0.174	817.3	0.007	4837.6	0.766	8141.1	~0.000
180	0.077	27.2	0.179	167.6	0.309	729.4	0.433	3901.2	~0.000

Table 6. Discrete relaxation spectrum parameters for PriMA-PGM derived from the 4-term Prony series fitting

Temp (°C)	G_0	τ_0 (s)	G_1	τ_1 (s)	G_2	τ_2 (s)	G_3	τ_3 (s)	G_∞
120	0.009	6.1	0.020	104.1	0.012	1301.6	0.103	16040.5	0.855
130	0.011	6.6	0.020	131.0	0.013	731.4	0.152	10551.9	0.806
140	0.020	7.0	0.030	94.2	0.040	1008.9	0.317	15406.1	0.610
150	0.031	22.3	0.024	411.6	0.045	931.2	0.438	9199.0	0.462
160	0.053	25.0	0.007	4837.6	0.174	817.3	0.766	8141.1	~0.000
180	0.077	27.2	0.179	167.6	0.309	729.4	0.433	3901.2	~0.000

The equilibrium modulus (G_∞) indicates the network's persistent solid-like fraction, which predictably collapses as temperature increases. However, the onset of this collapse is heavily dictated by molecular architecture. The densely cross-linked PriMA-PG250 retains a measurable G_∞ of 5.5% even at 180°C, actively resisting complete viscous flow. In contrast, the looser PriMA-PG700 and the PriMA-PGM networks achieve total viscous flow (G_∞ ~0) by 160°C and 200°C, respectively.

Concurrently, the discrete modulus fractions (G_0 through G_3) reveal how thermal energy redistributes internal stress. At lower temperatures, relaxation is overwhelmingly dominated by the slowest, highly entangled mode (G_3). As heat is applied, this dominance shifts rapidly toward the faster intermediate modes (e.g., G_1 and G_2), demonstrating that thermal energy successfully overcomes topological resistance, breaking down heavy entanglements into highly mobile segments capable of rapid transesterification.

Ultimately, this discrete modeling perfectly validates the activation energy (E_a) analysis; the structurally less restricted PEGDA-700 and PEGDMA networks reach fluid-like states much faster than the robust PEGDA-250 baseline, confirming their exceptional suitability for efficient high-temperature reprocessability.

4.10 Mechanical Properties; Tensile Stress-Strain Behavior

The macroscopic mechanical behavior of the networks under uniaxial tension was evaluated to understand the influence of the precursor architecture on the final material properties. The representative stress-strain curves and property values for the PriMA-PG250 and PriMA-PG700 formulations are presented in Figure 18a and Table 7.

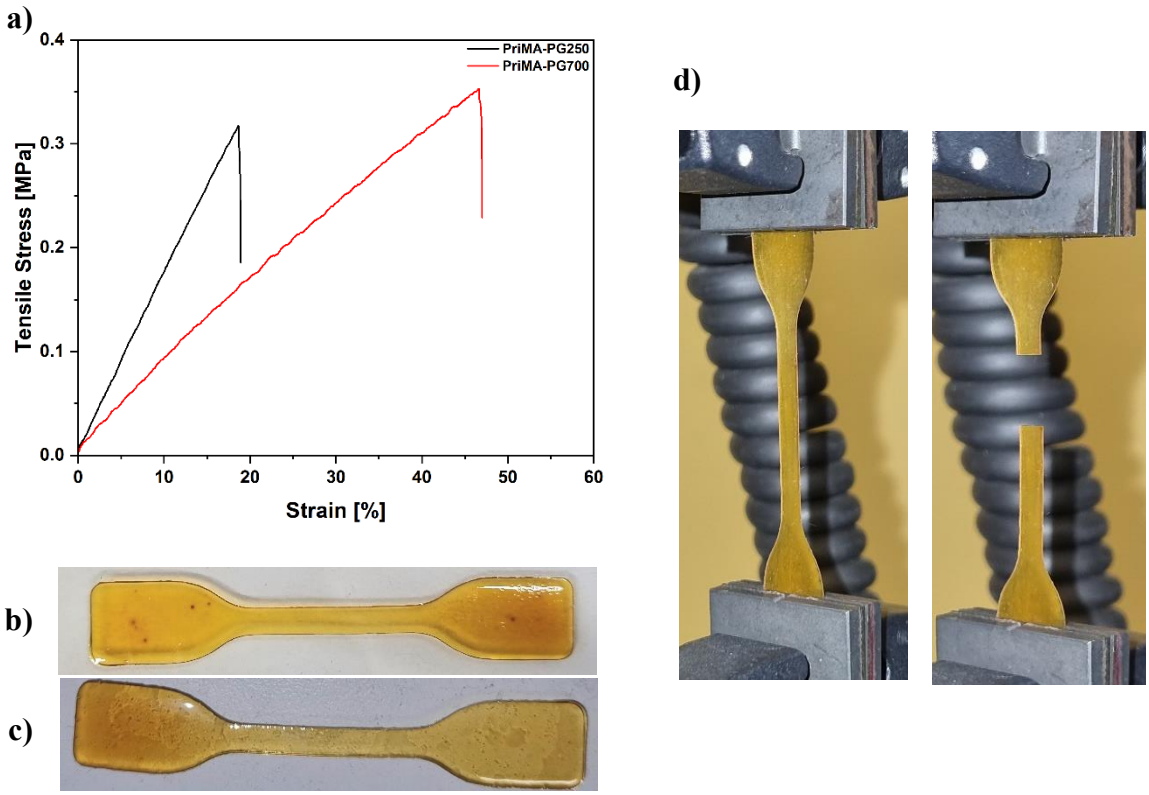

Figure 18. (a) Tensile stress-strain curves of the PriMA-PG250 (black line) and PriMA-PG700 (red line), (b) PriMA-PG250 sample, (c) PriMA-PG700 sample, (d) samples in the instrument before and after breaking

Table 7. mechanical properties of PriMA-PG250 and PriMA-PG700

Samples	Young's modulus [kPa]	maximum tensile stress [kPa]	elongation at break [%]	Toughness [kJ/m^3]
PriMA-PG250	17	320	19	3
PriMA-PG700	9	350	47	9

The PriMA-PG250 formulation exhibited stiffer, relatively less extensible behavior. It demonstrated a higher initial resistance to deformation, quantified by a Young's modulus of 0.017 MPa. The material reached a maximum tensile stress of approximately 0.32 MPa before experiencing failure at an elongation at break of around 19%. This behavior suggests a tighter, more rigid crosslinked network, which aligns with the use of shorter crosslinker segments.

The PriMA-PG700 formulation demonstrated significantly enhanced flexibility and stretching capacity. It displayed a lower initial stiffness, indicated by a reduced Young's modulus of 0.009 MPa. However, the material was strain-hardened to achieve a slightly higher maximum tensile stress of approximately 0.35 MPa. Most notably, the elongation

at break for the PriMA-PG700 network was higher, reaching ~ 47% before failure. This pronounced increase in ductility and the ability to undergo significant deformation can be directly attributed to the longer molecular chain length of the PG700 precursor. The longer segments between crosslinking points impart greater free volume and segmental mobility within the network, allowing the chains to unravel and align in the direction of the applied force before ultimately breaking.[79,80]

5 Conclusion

This study successfully demonstrates the design, synthesis, and systematic characterization of a novel class of catalyst-free, bio-based PBAE CANs. By integrating a customized, branched MATEOA monomer with a highly reactive Priamine 1071 donor and varying macromonomer, the fundamental structure-property relationships governing network formation, mechanical performance, and dynamic bond exchange were explained.

The investigation into structural variations revealed that both the steric hindrance of the reactive groups and the aliphatic chain length profoundly dictate the ultimate material properties. The incorporation of a methacrylic chain (PriMA-PGM) exposed critical kinetic limitations; the electron-donating and sterically bulky methyl group severely restricted nucleophilic attack, inducing premature vitrification and resulting in a highly defective, largely soluble macroscopic architecture (31.3% gel content).

Spectroscopic analysis via FTIR corroborated these structural developments, tracking the extent of the aza-Michael addition through the characteristic conversion of the α,β-unsaturated carbonyl stretching band (1720 cm^{-1}) into the saturated ester frequency (1740 cm^{-1}). Notably, the PriMA-PG700 formulation achieved the most robust functional group conversion (reaching 1.10 compared to 1.07 for PriMA-PG250). Furthermore, the extended macromonomers introduced distinct thermal advantages. Specifically, the increased molar mass and extended chain lengths of the PEGDA-700 and PEGDMA-750 macromonomers provided better thermal resistance by increasing the first onset temperature of degradation. This is vital as it establishes a broader, more stable thermal processing range of temperature, directly enabling safer and faster high-temperature reprocessability.

Despite the thermal advantages of the heavier macromonomers, the unhindered acrylate formulations yielded the most viable, structurally tunable networks. The baseline PriMA-PG250 formulation achieved the most optimal cross-linking density (84.1% gel fraction), characterized by Young's modulus of 17 kPa and relatively brittle failure at 19% elongation. Conversely, increasing the molecular weight of the macromonomer in (PriMA-PG700) effectively reduced the cross-link density, shifting the dynamic mechanical α-transition to a lower temperature (-43 °C). This expanded free volume fundamentally altered the macroscopic mechanical profile, transforming the stiff matrix into a highly extensible, rubber-like material capable of accommodating ~47% strain before failure. The longer crosslinker segments acted as an exceptionally toughening agent, effectively tripling the total energy absorption of the network to 9 kJ/m^3.

Crucially, Arrhenius activation energy (E_a) calculations and 4-term Prony series modeling explicitly linked the dynamic viscoelastic properties to the network topology. The PriMA-PG250 exhibited a high E_a (294.9 kJ/mol) and maintained a persistent solid-like modulus (G_∞ =5.5%) at 180 °C, actively resisting flow. The PriMA-PGM network displayed an intermediate activation barrier of 195.0 kJ/mol, inherently restricted by its kinetically trapped architecture. In contrast, the looser PriMA-PG700 required a significantly lower activation barrier (103.7 kJ/mol) and rapidly achieved total viscous flow (G_∞ ~0) by 160 °C. These results explicitly demonstrate that the longer crosslinker segment greatly facilitates network disentanglement and dynamic bond exchange, ultimately resulting in vastly superior thermal reprocessability of the final product.

Ultimately, this work establishes that the PBAE vitrimer platform is highly modular. While the PriMA-PG250 formulation provides an optimal balance of structural integrity and functional group conversion suitable for robust CAN applications, the enhanced chain mobility of the PEGDA-700 network makes it an exceptional candidate for applications requiring high ductility and rapid, efficient thermal reprocessability. These findings provide a vital predictive framework for engineering next-generation, sustainable, covalent adaptable networks tailored for specific processing and performance requirements, paving the way for future exploration into fully closed-loop recyclable composites and the industrial scaling of bio-based dynamic initial values.

6 Bibliography

(1) Taplan, C.; Guerre, M.; Du Prez, F. E. Covalent Adaptable Networks Using β-Amino Esters as Thermally Reversible Building Blocks. *J. Am. Chem. Soc.* **2021**, *143* (24), 9140–9150.

(2) Cuminet, F.; Caillol, S.; Dantras, É.; Leclerc, É.; Ladmiral, V. Neighboring Group Participation and Internal Catalysis Effects on Exchangeable Covalent Bonds: Application to the Thriving Field of Vitrimer Chemistry. *Macromolecules*. American Chemical Society May 11, 2021, pp 3927–3961.

(3) Patrick, J. F.; Robb, M. J.; Sottos, N. R.; Moore, J. S.; White, S. R. Polymers with Autonomous Life-Cycle Control. *Nature* **2016**, *540* (7633), 363–370.

(4) Maes, S.; Badi, N.; Winne, J. M.; Du Prez, F. E. Taking Dynamic Covalent Chemistry out of the Lab and into Reprocessable Industrial Thermosets. *Nat. Rev. Chem.* **2025**, *9* (3), 144–158.

(5) Denissen, W.; Winne, J. M.; Du Prez, F. E. Vitrimers: Permanent Organic Networks with Glass-like Fluidity. *Chem. Sci.* **2015**, *7* (1), 30–38.

(6) Kloxin, C. J.; Bowman, C. N. Covalent Adaptable Networks: Smart, Reconfigurable and Responsive Network Systems. *Chem. Soc. Rev.* **2013**, *42* (17), 7161–7173.

(7) Sun, M.; Felsenthal, L. M.; Kim, S.; Choi, E. Y.; Reed, L. J.; Elling, B. R.; Dichtel, W. R. Covalent Adaptable Networks: Reprocessable Cross-Linked Polymers. *Chem. Rev.* **2026**, *126* (3).

(8) Hakkarainen, M.; Xu, Y.; Odelius, K. Photocurable, Thermally Reprocessable, and Chemically Recyclable Vanillin-Based Imine Thermosets. *ACS Sustain. Chem. Eng.* **2020**, *8* (46), 17272–17279.

(9) Michal, B. T.; Jaye, C. A.; Spencer, E. J.; Rowan, S. J. Inherently Photohealable and Thermal Shape-Memory Polydisulfide Networks. *ACS Macro Lett.* **2013**, *2* (8), 694–699.

(10) Zhang, V.; Kang, B.; Accardo, J. V.; Kalow, J. A. Structure-Reactivity-Property Relationships in Covalent Adaptable Networks. *Journal of the American Chemical Society*. American Chemical Society December 14, 2022, pp 22358–22377.

(11) Stern, M. D.; Tobolsky, A. V.; Stern, M. D.; Tobolsky, A. V. Stress-Time-Temperature Relations in Polysulfide Rubbers. *Rubber Chemistry and Technology* **1946**, *19* (4), 1178–1192.

(12) Osthoff, R. C.; Bueche, A. M.; Grubb, W. T. Chemical Stress-Relaxation of Polydimethylsiloxane Elastomers1. *J. Am. Chem. Soc.* **2002**, *76* (18), 4659–4663.

(13) Scott, T. F.; Schneider, A. D.; Cook, W. D.; Bowman, C. N. Chemistry: Photoinduced Plasticity in Cross-Linked Polymers. *Science (1979).* **2005**, *308* (5728), 1615–1617.

(14) Chen, X.; Dam, M. A.; Ono, K.; Mal, A.; Shen, H.; Nutt, S. R.; Sheran, K.; Wudl, F. A Thermally Re-Mendable Cross-Linked Polymeric Material. *Science (1979).* **2002**, *295* (5560), 1698–1702.

(15) Terryn, S.; Brancart, J.; Lefeber, D.; Van Assche, G.; Vanderborght, B. Self-Healing Soft Pneumatic Robots. *Sci. Robot.* **2017**, *2* (9).

(16) Chapelle, C.; Quienne, B.; Bonneaud, C.; David, G.; Caillol, S. Diels-Alder-Chitosan Based Dissociative Covalent Adaptable Networks. *Carbohydr. Polym.* **2021**, *253* (12), 117222.

(17) Obadia, M. M.; Mudraboyina, B. P.; Serghei, A.; Montarnal, D.; Drockenmuller, E. Reprocessing and Recycling of Highly Cross-Linked Ion-Conducting Networks through Transalkylation Exchanges of C–N Bonds. *J. Am. Chem. Soc.* **2015**, *137* (18), 6078–6083.

(18) Obadia, M. M.; Jourdain, A.; Cassagnau, P.; Montarnal, D.; Drockenmuller, E. Tuning the Viscosity Profile of Ionic Vitrimers Incorporating 1,2,3-Triazolium Cross-Links. *Adv. Funct. Mater.* **2017**, *27* (45).

(19) Hendriks, B.; Waelkens, J.; Winne, J. M.; Du Prez, F. E. Poly(Thioether) Vitrimers via Transalkylation of Trialkylsulfonium Salts. *ACS Macro Lett.* **2017**, *6* (9), 930–934.

(20) Capelot, M.; Montarnal, D.; Tournilhac, F.; Leibler, L. Metal-Catalyzed Transesterification for Healing and Assembling of Thermosets. *J. Am. Chem. Soc.* **2012**, *134* (18), 7664–7667.

(21) Wang, C.; Goldman, T. M.; Worrell, B. T.; McBride, M. K.; Alim, M. D.; Bowman, C. N. Recyclable and Repolymerizable Thiol–X Photopolymers. *Mater. Horiz.* **2018**, *5* (6), 1042–1046.

(22) Montarnal, D.; Capelot, M.; Tournilhac, F.; Leibler, L. Silica-like Malleable Materials from Permanent Organic Networks. *Science* **2011**, *334* (6058), 965–968.

(23) Guerre, M.; Taplan, C.; Nicolaÿ, R.; Winne, J. M.; Du Prez, F. E. Fluorinated Vitrimer Elastomers with a Dual Temperature Response. *J. Am. Chem. Soc.* **2018**, *140* (41), 13272–13284.

(24) Denissen, W.; Rivero, G.; Nicolaÿ, R.; Leibler, L.; Winne, J. M.; Du Prez, F. E. Vinylogous Urethane Vitrimers. *Adv. Funct. Mater.* **2015**, *25* (16), 2451–2457.

(25) Taplan, C.; Guerre, M.; Winne, J. M.; Du Prez, F. E. Fast Processing of Highly Crosslinked, Low-Viscosity Vitrimers. *Mater. Horiz.* **2020**, *7* (1), 104–110.

(26) Taynton, P.; Ni, H.; Zhu, C.; Yu, K.; Loob, S.; Jin, Y.; Qi, H. J.; Zhang, W. Repairable Woven Carbon Fiber Composites with Full Recyclability Enabled by Malleable Polyimine Networks. *Advanced Materials* **2016**, *28* (15), 2904–2909.

(27) Whiteley, J. M.; Taynton, P.; Zhang, W.; Lee, S. H. Ultra-Thin Solid-State Li-Ion Electrolyte Membrane Facilitated by a Self-Healing Polymer Matrix. *Advanced Materials* **2015**, *27* (43), 6922–6927.

(28) Taplan, C.; Guerre, M.; Bowman, C. N.; Du Prez, F. E. Surface Modification of (Non)-Fluorinated Vitrimers through Dynamic Transamination. *Macromol. Rapid Commun.* **2021**, *42* (7).

(29) Liu, J.; Liu, X.; Cui, X.; Qin, J.; Shi, M.; Wang, D.; Liang, L.; Yang, C.; Liu, J.; Liu, X.; Cui, X.; Qin, J.; Shi, M.; Wang, D.; Liang, L.; Yang, C.; Liu; Jiaming; Liu; Xiaohong; Cui; Xiaohua; Qin; Jingjing; Shi; Min; Wang; Dingsong; Liang; Liyan; Yang; Chaolong. Imine-Containing Epoxy Vitrimer Cured by Active Ester: Properties and Theoretical Analysis. *AAPM* **2023**, *5* (12), 10042–10052.

(30) Sölle, B.; Schmallegger, M.; Schlögl, S.; Rossegger, E. Wavelength-Dependent Dynamic Behavior in Thiol-Ene Networks Based on Disulfide Exchange. *J. Am. Chem. Soc.* **2024**, *146* (49), 34152–34157.

(31) Lee, G.; Song, H. Y.; Choi, S.; Kim, C. Bin; Hyun, K.; Ahn, S. K. Harnessing β-Hydroxyl Groups in Poly(β-Amino Esters) toward Robust and Fast Reprocessing Covalent Adaptable Networks. *Macromolecules* **2022**, *55* (23), 10366–10376.

(32) Scheutz, G. M.; Lessard, J. J.; Sims, M. B.; Sumerlin, B. S. Adaptable Crosslinks in Polymeric Materials: Resolving the Intersection of Thermoplastics and Thermosets. *J. Am. Chem. Soc.* **2019**, *141* (41), 16181–16196.

(33) Ying, H.; Zhang, Y.; Cheng, J. Dynamic Urea Bond for the Design of Reversible and Self-Healing Polymers. *Nature Communications 2014 5:1* **2014**, *5* (1), 3218-.

(34) Zhang, X.; Wang, S.; Jiang, Z.; Li, Y.; Jing, X. Boronic Ester Based Vitrimers with Enhanced Stability via Internal Boron-Nitrogen Coordination. *J. Am. Chem. Soc.* **2020**, *142* (52), 21852–21860.

(35) Baruah, R.; Kumar, A.; Ujjwal, R. R.; Kedia, S.; Ranjan, A.; Ojha, U. Recyclable Thermosets Based on Dynamic Amidation and Aza-Michael Addition Chemistry. *Macromolecules* **2016**, *49* (20), 7814–7824.

(36) Zhang, B.; Digby, Z. A.; Flum, J. A.; Chakma, P.; Saul, J. M.; Sparks, J. L.; Konkolewicz, D. Dynamic Thiol–Michael Chemistry for Thermoresponsive Rehealable and Malleable Networks. *Macromolecules* **2016**, *49* (18), 6871–6878.

(37) Kleine, T. S.; Nguyen, N. A.; Anderson, L. E.; Namnabat, S.; Lavilla, E. A.; Showghi, S. A.; Dirlam, P. T.; Arrington, C. B.; Manchester, M. S.; Schwiegerling, J.; Glass, R. S.; Char, K.; Norwood, R. A.; Mackay, M. E.; Pyun, J. High Refractive Index Copolymers with Improved Thermomechanical Properties via the Inverse Vulcanization of Sulfur and 1,3,5-Triisopropenylbenzene. *ACS Macro Lett.* **2016**, *5* (10), 1152–1156.

(38) Liu, W. X.; Zhang, C.; Zhang, H.; Zhao, N.; Yu, Z. X.; Xu, J. Oxime-Based and Catalyst-Free Dynamic Covalent Polyurethanes. *J. Am. Chem. Soc.* **2017**, *139* (25), 8678–8684.

(39) Alabiso, W.; Schlögl, S. The Impact of Vitrimers on the Industry of the Future: Chemistry, Properties and Sustainable Forward-Looking Applications. *Polymers 2020, Vol. 12,* **2020**, *12* (8).

(40) Delahaye, M.; Tanini, F.; Holloway, J. O.; Winne, J. M.; Du Prez, F. E. Double Neighbouring Group Participation for Ultrafast Exchange in Phthalate Monoester Networks. *Polym. Chem.* **2020**, *11* (32), 5207–5215.

(41) Liu, Y.; Li, Y.; Keskin, D.; Shi, L. Poly(β-Amino Esters): Synthesis, Formulations, and Their Biomedical Applications. *Adv. Healthc. Mater.* **2019**, *8* (2), 1801359.

(42) Yu. Rulev, A. Aza-Michael Reaction: A Decade Later – Is the Research Over? *European J. Org. Chem.* **2023**, *26* (26), e202300451.

(43) Nguyen, L. T.; Mertens, C.; Du Prez, F. E. Aza-Michael Chemistry for PDMS-Based Covalent Adaptable Elastomers: Design and Dual Role of the Silica Filler. *Macromolecules* **2024**, *57* (10), 4817–4825.

(44) Anderson, D. G.; Tweedie, C. A.; Hossain, N.; Navarro, S. M.; Brey, D. M.; Van Vliet, K. J.; Langer, R.; Burdick, J. A. A Combinatorial Library of Photocrosslinkable and Degradable Materials. *Advanced Materials* **2006**, *18* (19), 2614–2618.

(45) Cuminet, F.; Caillol, S.; Dantras, É.; Leclerc, É.; Ladmiral, V. Neighboring Group Participation and Internal Catalysis Effects on Exchangeable Covalent Bonds: Application to the Thriving Field of Vitrimer Chemistry. *Macromolecules* **2021**, *54* (9), 3927–3961.

(46) Ecochard, Y.; Auvergne, R.; Boutevin, B.; Caillol, S. Linseed Oil-Based Thermosets by Aza-Michael Polymerization. *European Journal of Lipid Science and Technology* **2020**, *122* (1), 1900145.

(47) Altuna, F. I.; Hoppe, C. E.; Williams, R. J. J. Epoxy Vitrimers with a Covalently Bonded Tertiary Amine as Catalyst of the Transesterification Reaction. *Eur. Polym. J.* **2019**, *113* (6058), 297–304.

(48) Liu, Y.; Yu, Z.; Xu, X.; Wang, B.; Feng, H.; Li, P.; Zhu, J.; Ma, S. Crystallizable Aliphatic Chains Enhanced Covalent Adaptable Networks: Fast Reprocessing and Improved Performance. *Macromol. Rapid Commun.* **2022**, *43* (20), 2200379.

(49) Dugas, L. D.; Walker, W. D.; Shankar, R.; Hoppmeyer, K. S.; Thornell, T. L.; Morgan, S. E.; Storey, R. F.; Patton, D. L.; Simon, Y. C.; Dugas, L. D.; Walker [+], W. D.; Shankar, R.; Hoppmeyer, K. S.; Morgan, S. E.; Storey, R. F.; Patton, D. L.; Simon, Y. C.; Thornell, T. L. Diketoenamine-Based Vitrimers via Thiol-Ene Photopolymerization. *Macromol. Rapid Commun.* **2022**, *43* (24), 2200249.

(50) Test Methods for Determination of Gel Content and Swell Ratio of Crosslinked Ethylene Plastics. **2016**.

(51) Redmann, A.; Oehlmann, P.; Scheffler, T.; Kagermeier, L.; Osswald, T. A. Thermal Curing Kinetics Optimization of Epoxy Resin in Digital Light Synthesis. *Addit. Manuf.* **2020**, *32* (6228), 101018.

(52) Sun Han Chang, R.; Lee, J. C. W.; Pedron, S.; Harley, B. A. C.; Rogers, S. A. Rheological Analysis of the Gelation Kinetics of an Enzyme Cross-Linked PEG Hydrogel. *Biomacromolecules* **2019**, *20* (6), 2198–2206.

(53) Pascault, J.-P.; Sautereau, H.; Verdu, J.; Williams, R. J. J. Thermosetting Polymers. *Thermosetting Polymers* **2002**.

(54) Azizi, N.; Saidi, M. R. LiClO4 Accelerated Michael Addition of Amines to α,β-Unsaturated Olefins under Solvent-Free Conditions. *Tetrahedron* **2004**, *60* (2), 383–387.

(55) Chaudhuri, M. K.; Hussain, S.; Kantam, M. L.; Neelima, B. Boric Acid: A Novel and Safe Catalyst for Aza-Michael Reactions in Water. *Tetrahedron Lett.* **2005**, *46* (48), 8329–8331.

(56) Ranu, B. C.; Banerjee, S. Significant Rate Acceleration of the Aza-Michael Reaction in Water. *Tetrahedron Lett.* **2007**, *48* (1), 141–143.

(57) Escalante, J.; Carrillo-Morales, M.; Linzaga, I. Michael Additions of Amines to Methyl Acrylates Promoted by Microwave Irradiation. *Molecules 2008, Vol. 13, Pages 340-347* **2008**, *13* (2), 340–347.

(58) Jenner, G. Catalytic High Pressure Synthesis of Hindered β-Aminoesters. *Tetrahedron Lett.* **1995**, *36* (2), 233–236.

(59) Achilias, D. S.; Karabela, M. M.; Sideridou, I. D. Thermal Degradation and Isoconversional Kinetic Analysis of Light-Cured Dimethacrylate Copolymers. *J. Therm. Anal. Calorim.* **2010**, *99* (3), 917–923.

(60) Socrates, G. Infrared and Raman Characteristic Group Frequencies. Tables and Charts. *Journal of Raman Spectroscopy* **2001**, 347.

(61) Noordzij, G. J.; Wilsens, C. H. R. M. Cascade Aza-Michael Addition-Cyclizations; Toward Renewable and Multifunctional Carboxylic Acids for Melt-Polycondensation. *Front. Chem.* **2019**, *7*.

(62) Flory, P. J. Molecular Theory of Rubber Elasticity. *Polym. J.* **1985**, *17* (1), 1–12.

(63) Schoff, C. K. Dynamic Mechanical Analysis. *CoatingsTech* **2008**, *5* (10), 44.

(64) Keim, T.; Gall, K. Synthesis, Characterization, and Cyclic Stress-Influenced Degradation of a Poly(Ethylene Glycol)-Based Poly(Beta-Amino Ester). *J. Biomed. Mater. Res. A* **2010**, *92* (2), 702–711.

(65) Kowalczyk, A.; Kraśkiewicz, A.; Weisbrodt, M.; Kowalczyk, K. Hydrogels Based on Poly(2-Hydroxyethyl Methacrylate) and Nettle Extract. *Polimery* **2023**, *68* (9), 461–472.

(66) Wellen, R. M. R.; Canedo, E.; Rabello, M. S. Nonisothermal Cold Crystallization of Poly(Ethylene Terephthalate). *Journal of Materials Research 2011 26:9* **2011**, *26* (9), 1107–1115.

(67) Mantala, K.; Crespy, D. Requirements for Achieving Self-Healing at Low/Room Temperature in Polymers. *Macromolecules* **2025**, *58* (20), 10986.

(68) Lin, C. C.; Anseth, K. S. PEG Hydrogels for the Controlled Release of Biomolecules in Regenerative Medicine. *Pharm. Res.* **2008**, *26* (3), 631.

(69) Rydholm, A. E.; Reddy, S. K.; Anseth, K. S.; Bowman, C. N. Controlling Network Structure in Degradable Thiol−Acrylate Biomaterials to Tune Mass Loss Behavior. *Biomacromolecules* **2006**, *7* (10), 2827–2836.

(70) Capelot, M.; Unterlass, M. M.; Tournilhac, F.; Leibler, L. Catalytic Control of the Vitrimer Glass Transition. *ACS Macro Lett.* **2012**, *1* (7), 789–792.

(71) Ricarte, R. G.; Shanbhag, S. A Tutorial Review of Linear Rheology for Polymer Chemists: Basics and Best Practices for Covalent Adaptable Networks. *Polym. Chem.* **2024**, *15* (9), 815–846.

(72) Bao, C.; Yin, Y.; Ding, Y.; Liu, J.; Xu, Y.; Miao, R.; Liu, Z.; Duan, B.; Qin, Y.; Xin, Z. Chemically Recyclable Supramolecular Thermosets toward Strong and Reusable Hot-Melt Adhesives. *Macromolecules* **2023**, *56* (17), 6633–6643.

(73) Ferry, J.; Society, H. M.-J. of T. E.; 1961, undefined. Viscoelastic Properties of Polymers. *iopscience.iop.orgJD Ferry, HS MyersJournal of The Electrochemical Society, 1961•iopscience.iop.org* **1980**.

(74) Hotta, A.; Clarke, S. M.; Terentjev, E. M. Stress Relaxation in Transient Networks of Symmetric Triblock Styrene−Isoprene−Styrene Copolymer. *Macromolecules* **2001**, *35* (1), 271–277.

(75) Jourdain, A.; Asbai, R.; Anaya, O.; Chehimi, M. M.; Drockenmuller, E.; Montarnal, D. Rheological Properties of Covalent Adaptable Networks with 1,2,3-Triazolium Cross-Links: The Missing Link between Vitrimers and Dissociative Networks. *Macromolecules* **2020**, *53* (6), 1884–1900.

(76) Han, J.; Liu, T.; Hao, C.; Zhang, S.; Guo, B.; Zhang, J. A Catalyst-Free Epoxy Vitrimer System Based on Multifunctional Hyperbranched Polymer. *Macromolecules* **2018**, *51* (17), 6789–6799.

(77) Hayashi, M. Dominant Factor of Bond-Exchange Rate for Catalyst-Free Polyester Vitrimers with Internal Tertiary Amine Moieties. *ACS Appl. Polym. Mater.* **2020**, *2* (12), 5365–5370.

(78) Williams, G.; Watts, D. C. Non-Symmetrical Dielectric Relaxation Behaviour Arising from a Simple Empirical Decay Function. *Transactions of the Faraday Society* **1970**, *66* (0), 80–85.

(79) Hassan, M. K.; Tucker, S. J.; Abukmail, A.; Wiggins, J. S.; Mauritz, K. A.; Hassan, M. K.; Tucker, S. J.; Abukmail, A.; Wiggins, J. S.; Mauritz, K. A. Polymer Chain Dynamics in Epoxy Based Composites as Investigated by Broadband Dielectric Spectroscopy. *Arabian Journal of Chemistry* **2016**, *9* (2), 305–315.

(80) Stern, T. Single-Step Synthesis and Characterization of Non-Linear Tough and Strong Segmented Polyurethane Elastomer Consisting of Very Short Hard and Soft Segments and Hierarchical Side-Reacted Networks and Single-Step Synthesis of Hierarchical Hyper-Branched Pol…. *Molecules 2024, Vol. 29,* **2024**, *29* (7).